Final Report
(June, 1996)

"Trace Element Abundance Measurements on Cosmic Dust Particles"

The X-Ray Microprobe on beamline X-26A at the National Synchrotron Light Source (NSLS) at Brookhaven National Laboratory was used to determine the abundances of elements from Cr through Sr in individual interplanetary dust particles (IDPs) collected from the Earth's stratosphere and the Scanning Transmission X-ray Microscope (STXM) on beamline X-1A at the NSLS was used to determine the carbon abundances and spatial distributions in IDPs. In addition, modeling was performed in an attempt to associate particular types of IDPs with specific types of parent bodies, and thus to infer the chemistry, mineralogy, and structural properties of those parent bodies.

Chemical Analyses of IDPs

The IDPs collected from the Earth's stratosphere are separated by the collection process into two groups: those which survive collection intact (presumably structurally strong) and those which break up into numerous fragments on collection (called "cluster particles," which are presumably structurally weaker than the IDPs collected intact). Since the carbonaceous meteorites exhibit clear chemical trends which correlate with structural strength, with the weakest CI chondrites having the highest concentrations of the volatile elements, we have focused on determining if there are similar chemical differences between these two groups of IDPs.

We reported on the measurement of element abundances in large IDPs collected intact in Appendix B and the chemical compositions of fragments from cluster IDPs in Appendix F. The results provide the first indication that the weaker cluster fragments are volatile rich compared to the CI meteorites while the group of large, stronger IDPs collected intact have volatile contents roughly comparable to the CI meteorites. This suggests a continuation of the chemical trend previously observed in meteorites, with the extremely weak cluster IDPs being even more volatile rich than the CI meteorites.

We conducted a comprehensive study of the chemical composition of the small IDPs, undertaken in collaboration with Dr. M. Zolensky (NASA JSC) and K. L. Thomas (Lockheed), who measured the abundances of volatile major elements in the IDPs. These results (in Appendix M) demonstrate that not only are the volatile trace elements measured using the X-ray Microprobe (Cu, Zn, Ga, Ge, Se, and Br) enriched relative to CI in these IDPs, but that there are enrichments of the same magnitude (about a factor of 3) in the volatile major elements Na, K, and P as well as carbon. Only S, among the volatile elements measured in this study, is not enriched relative to CI, and this may be a result of atmospheric entry heating.

CONCLUSIONS: *These results indicate that some of the IDPs sample a new type of extraterrestrial material, structurally weaker and more volatile-rich than the weakest and most volatile-rich meteorites (the CI carbonaceous chondrites).*

Carbon Analyses

Carbon is a particularly important element in the IDPs for two reasons. First, carbon has the lowest nebula condensation temperature of the elements studied in Appendix M (Fegley, 1994), thus carbon may provide a particularly sensitive indicator of the temperature of dust formation in the solar nebula. Second, Anders (Nature, 1989) has pointed out that IDPs may have contributed a significant pre-biotic organic matter to the early surface of the Earth, and that this organic matter may have played an important role in the origin of life.

Previous carbon measurements in the IDPs were performed by fluorescence analysis (Schramm et al., 1989; Thomas et al., 1994), a technique which is hampered by the small escape depth for carbon K-x-rays. This means that all fluorescence-based carbon measurements on whole IDPs really measure the carbon in only a thin surface layer, and the actual abundance of

carbon in the sample is quite uncertain, depending critically on whether the carbon occurs in a surface layer or is distributed homogeneously throughout the sample. The actual spatial distribution of carbon is not measured in the fluorescence analysis, thus it is uncertain how the data should be reduced.

We have used the Scanning Transmission X-ray Microscope (STXM) at the NSLS to determine the carbon abundances in ultra-microtome thin sections of IDPs. This technique provides a map of the spatial distribution of the carbon in each section, measures the bulk carbon content of the section, and further provides the opportunity to determine the carbon bonding state at specific points on the section. The instrument, and the first carbon results on three IDPs, are described in Appendix C and Appendix H.

CONCLUSIONS: *These results confirm that the high carbon contents of IDPs, previously reported by the fluorescence technique, are correct. Further the STXM provides maps showing the spatial distribution of carbon in each sample, something not available using the fluorescence analysis.*

Possible Br Contamination

The Br content of IDPs has always been puzzling, because most of the volatile elements are enriched by factors of 2 to 4 in the IDPs but Br is typically enriched by a factor of 10 to 100 (see Appendix M). We performed time-sequential measurements of the Br content of 6 large IDPs, and demonstrated that the Br content decreased with increasing exposure time in the x-ray beam.

CONCLUSIONS: *These results (shown in Appendix I) demonstrate that some of the Br in the IDPs is extremely weakly bound, possibly an indication that Br from the stratosphere has accreted onto the surface of the IDPs during their residence in the stratosphere. Although Br was lost from these particles, none of the other volatile trace elements decreased in abundance, suggesting that if the Br is a contaminant the other volatile trace elements do not experience similar contamination.*

Properties of the Asteroids as Inferred from the IDPs

The interplanetary dust particles provide the opportunity to study the physical, chemical, and mineralogical properties of their parent bodies (asteroids and comets), providing information useful in the design of future sample return missions. The IDPs sample all of the sources of dust in the solar system, but Earth gravitational focusing strongly biases the IDPs collected from the Earth's stratosphere in favor of particles from sources with low inclinations and eccentricities (Flynn, 1989). This biases the stratospheric IDPs in favor of asteroidal rather than cometary IDPs. Following up on that, modeling by Kortenkamp et al. (1996) has shown that dust from the Themis and Koronis families of asteroids, two of the asteroid families thought to have produced dust bands detected by the IRAS satellite, should produce about 55% of all the IDPs collected at Earth.

The Koronis family of asteroids is particularly interesting, since this family consists of asteroids classified as S-type based on their reflection spectra. S-type asteroids are the most common type of asteroid in the inner region of the main-belt. The S-type asteroids are unusual in that no meteorite in the collections matches the reflection spectra of the S-type asteroids, thus the properties of these S-type asteroids are not known. Some investigators have suggested that the S-type asteroids are the source of the ordinary chondrite meteorites, speculating that the difference in reflection characteristics is due to "space weathering" of the exposed surfaces of the asteroids.

CONCLUSION: *We concluded (in Appendix J) that if the modeling by Kortenkamp et al. (1996) is correct, then the absence of ordinary chondrite material among the IDPs indicates the Koronis family of S-type asteroids is not similar in chemical composition to ordinary chondrites.*

Development of an "In-Situ" Analysis Technique for Particles Captured in Aerogel

Interplanetary dust particles have been captured in aerogel collectors flown on the Space Shuttle and on the Russian MIR Space Station. Preliminary analyses of particles removed from the Space Shuttle collectors (Tsou et al., 1993) found only orbital debris particles. The removal of a single particle from the aerogel is a tedious, time-consuming process. We have developed a quick screening technique, to distinguish space debris from chondritic IDPs without removing them from the aerogel. We use the X-Ray Microprobe to detect the fluorescence from major elements in each captured particle, and to classify each particle as man-made space debris or interplanetary dust based on its composition. A similar classification technique is used by the Johnson Space Center Curatorial Facility to separate the material colleced from the Earth's stratosphere into cosmic, natural terrestrial contamination, and man-made terrestrial contamination. However, prior to our development of the in-situ analysis technique, particles collected in aerogel on space missions required tedious removal of each particle from the aerogel prior to chemical analysis and classification.

CONCLUSIONS: *We demonstrated that in-situ measurement of the Ni/Fe ratios of captured particles provides a convenient distinction between chondritic particles and most types of space debris, allowing quick screening of particles captured using aerogel collectors on the Space Shuttle, the MIR Space Station or free-flying satellites (see Appendix K). This technique will also allow rapid preliminary characterization of the comet samples to be returned to Earth by NASA's planned STARDUST Discovery mission.*

Appendix A:

Appendix A: Flynn, G.J. (1995) Atmospheric Entry Heating of Large Interplanetary Dust, (abstract) Meteoritics, 30, 504-505.

ATMOSPHERIC ENTRY HEATING OF LARGE INTERPLANETARY DUST PARTICLES. G. J. Flynn, Department of Physics, State University of New York, Plattsburgh NY 12901, USA.

Large (>35 μm) interplanetary dust particles (IDPs) collected from the Earth's stratosphere are less severely heated during atmospheric entry, on average, than predicted. Evidence of severe heating, i.e., magnetite rims, high He-release temperatures, and Zn depletions, is found in a substantial fraction (~20–50%) of the small IDPs (10–20 μm) from the stratospheric collections. Larger IDPs having the same density and velocity distribution should be more severely heated during atmospheric entry. However, Flynn et al. [1,2] found low Zn contents in only 2 of 13 (15%) large IDPs. All four of these 13 IDPs examined thus far by TEM showed no magnetite rims [1]. Since these large IDPs generally appear to be less porous than the smaller IDPs, the observation that a lesser fraction is severely heated suggests the large IDPs have a lower mean atmospheric entry velocity than the smaller IDPs.

TABLE 1. Fraction of incident particles vs. peak temperature.

	Atmospheric Entry Velocity (km/s)				
Peak Temp.	11.1	12	13	14	15
<1300 K	0.82	0.52	0.32	0.20	0.14
>1300 K	0.18	0.48	0.68	0.80	0.86
>1600 K	0	0	0	0	0.28
Ratio*	0.2	0.9	2.1	4.0	4.1
	Atmospheric Entry Velocity (km/sec)				
	16	17	18	19	
<1300 K	0.09	0.06	0.05	0.03	
>1300 K	0.91	0.94	0.95	0.97	
>1600 K	0.52	0.66	0.76	0.83	
Ratio*	4.3	4.7	4.4	4.3	

* Ratio of IDPs heated between 1300 K and 1600 K to those not heated above 1300 K.

Pulse-heating experiments on 50–100-μm fragments of CI meteorite matrix demonstrate the onset of Zn loss by about 1300 K [3,4], well below the 1600 K melting temperature of anhydrous silicates. For the 13 large IDPs the ratio of those heated between 1300 K and 1600 K (i.e., unmelted but showing Zn loss) to those not heated to 1300 K is 2.11 ± 0.18.

The entry heating of large IDPs was modeled using the equations developed by Fraundorf [5] for the case of minimum entry velocity, 11.1 km/s (Earth escape velocity from 100 km), and for higher velocities in 1 km/s steps. IDPs were modeled as 36-μm spheres having a density of 2 g cc (consistent with the compact structure of large IDPs). Table 1 shows the fraction not heated above 1300 K, the fraction heated above 1300 K, and the fraction heated above 1600 K. The last line of the table is the ratio between the number of particles heated between 1300 K and 1600 K and those heated below 1300 K. This ratio is very low (0.20) for the minimum entry velocity case, but increases rapidly to 2.1 as the entry velocity increases to 13 km/s. The ratio then becomes almost constant, varying between 4 and 5 as the entry velocity increases to 19 km/s, reflecting the loss of the most severely heated particles by melting.

The ratio (0.18) observed for the 13 large IDPs is only consistent with an entry velocity distribution sharply peaked near 11.1 km/s. This is different from the velocity distributions measured for radar and photographic meteors, which have mean values of 15 to >18 km/s [6]. More detailed consideration of the shapes of large IDPs is required, but the high fraction of large IDPs showing no indication of severe entry heating suggests a source with extremely low geocentric velocity, most likely main-belt asteroids, with little or no contribution from sources giving higher Earth encounter velocities.

References: [1] Flynn G. J. et al. (1995) *LPS XXVI*, 407–408. [2] Flynn G. J. et al., this volume. [3] Klock W. et al. (1994) *LPS XXV*, 713–714. [4] Greshake A. et al. (1994) *Meteoritics*, *29*, 470. [5] Fraundorf P. (1980) *GRL*, *10*, 765–768. [6] Hughes D. W. (1978) in *Cosmic Dust*, 123–185, Wiley.

Appendix B:

Flynn, G.J., Bajt, S., Sutton, S.R., and Klock, W. (1995) Large Stratospheric IDPs: Chemical Composition and Comparison with Smaller Stratospheric IDPs, (abstract) Meteoritics, 30, 505.

LARGE STRATOSPHERIC IDPs: CHEMICAL COMPOSITION AND COMPARISON WITH SMALLER STRATOSPHERIC IDPs.
G. J. Flynn[1], S. Bajt[2], S. R. Sutton[2], and W. Klock[3]. [1]Department of Physics, State University of New York, Plattsburgh NY 12901, USA. [2]Department of Geophysical Sciences, University of Chicago, Chicago IL 60637,USA. [3]University of Halle, Halle, Germany.

Six large stratospheric IDPs, each greater than 35 μm, previously analyzed using the X-ray microprobe at the National Synchrotron Light Source showed an average volatile content consistent with CI or CM meteorites [1]. Seven additional large IDPs, ranging from 37 × 33 to 50 × 44 μm in size and having chondritic major-element abundances, have been analyzed using the same instrument. Each of these seven IDPs is depleted in Ca compared to CI (avg. Ca = 0.48× CI), a feature also observed in the first set of six, suggesting most or all of these IDPs are hydrated. The average trace-element content of these seven large IDPs is similar to the previous set of six (see Fig. 1), although Mn and Cu are about 70% higher in this set. The average composition of these large IDPs is distinctly different from that of smaller IDPs (generally 10–20 μm), which show enrichments of the volatiles Cu, Zn, Ga, Ge, and Se by factors of 1.5–3 over CI [2]. This suggests large IDPs that are strong enough to resist fragmentation on collection are chemically different from typical smaller IDPs. This may reflect a difference in the source(s) being sampled by the two types of IDPs. A subgroup of the smaller IDPs (9 of 51 particles) have a composition similar to CI meteorites and these large IDPs [2].

Bromine is enriched in most of these large IDPs. Two Br-rich IDPs (Br >300 ppm) and one Br-poor IDP (Br ~5 ppm) were each analyzed twice. The two Br-rich IDPs showed about a factor of 2 Br loss between the first and second analyses, presumably due to sample heating during the first analysis. This suggests some of the Br is very weakly bound in these Br-rich IDPs, a possible signature of Br surface contamination. However, the Br contents measured in the second analyses were still ~50× CI. No loss of Cu, Zn, Ga, Ge, or Se was detected in these IDPs, suggesting these elements are in more retentive sites. The Br-poor IDP (Br ~1.5× CI) showed no Br loss in the second analysis. Only one of these IDPs, L2008G10, showed a large Zn depletion (Zn/Fe <0.01× CI). This was accompanied by low contents of Ga, Ge, and Br (see Fig. 1). This pattern of Zn, Ge, Br, and Ga depletions was previously seen in smaller IDPs that were severely heated, presumably on atmospheric entry [2]. Sulfur and K are also low in L2008G10, suggesting these elements are also lost during heating, but the Se content is 0.8× CI. A second particle, L2009C8, has a Zn/Fe = 0.26× CI, possibly indicating less-severe heating. The low fraction of severely heated IDPs, only one in this set of seven and none in the set of six [1], suggests a very low atmospheric entry velocity for these large IDPs [3].

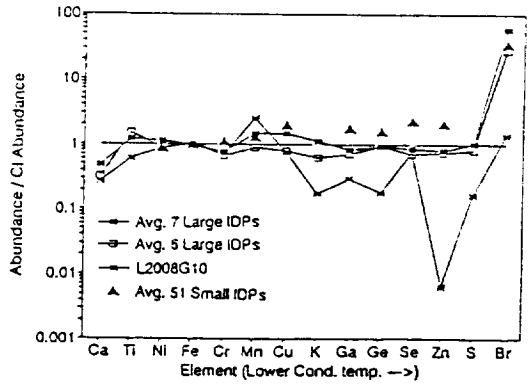

Fig. 1. Average Fe- and CI-normalized element abundances in 7 large IDPs, 6 different large IDPs [1], 51 smaller IDPs [2], and the single low-Zn IDP, L2008G10, included in the set of 7 large IDPs.

References: [1] Flynn G. J. et al. (1995) *LPS XXVI*, 407–408. [2] Flynn G. J. et al. (1993) *LPS XXIV*, 495–496. [3] Flynn G. J., this volume.

Appendix C:

Chapman, H.N., Bajt, S., Flynn, G.J., and Keller, L.P. (1995) Carbon Mapping and Carbon-XANES Measurements on an Interplanetary Dust Particle Using a Scanning Transmission X-Ray Microscope, (abstract) Meteoritics, 30, 496-497.

CARBON MAPPING AND CARBON-XANES MEASUREMENTS ON AN INTERPLANETARY DUST PARTICLE USING A SCANNING TRANSMISSION X-RAY MICROSCOPE. H. N. Chapman[1], S. Bajt[2], G. J. Flynn[3], and L. P. Keller[4], [1]State University of New York, Stony Brook NY 11794, USA, [2]The University of Chicago, IL 60637, USA, [3]State University of New York, Plattsburgh NY 12901, USA, [4]MVA, Inc., 5500-200 Oakbrook Parkway, Norcross GA 30093, USA.

The nature and distribution of C in interplanetary dust particles (IDPs) are important because C from IDPs has been proposed as a major source of prebiotic organic material on the early Earth [1] and may have been equally important on the surface of early Mars [2]; thus both the abundance and the types of C in IDPs have exobiology implications.

An ~12-μm chondritic-porous IDP (L2008F4) was embedded in S and thin sections (~50–80 μm thick) were prepared by ultramicrotomy. The thin sections were supported on SiO membranes and analyzed using the scanning transmission X-ray microscope (STXM) at the National Synchrotron Light Source, Brookhaven National Laboratory [3]. This microscope operates by focusing monochromatic X-rays to a 50-nm-diameter spot, through which the specimen is scanned, and detecting the flux transmitted through the specimen. The focusing lens is a zone plate, which operates efficiently over the range from 2.0 to 5.0 nm (250–600 eV). At the C edge, where this analysis was done, the flux on the sample is typically 1×10^6 photons/s for a 0.2-eV energy resolution.

High-resolution images (200 × 300 pixels over an area of 10 × 15 μm) of the IDP section were taken at energies of 281.8 eV and 302.4 eV, which are respectively below and above the C K-edge. Above the edge, C absorbs strongly, while it is virtually transparent at energies below the edge. By taking differences in the logarithm of the intensity at each pixel, maps proportional to the C density were obtained. The C mapping indicated that the thin section contains an estimated 34 vol% C.

The bonding state of C can be inferred from the X-ray absorption near-edge structure (XANES) [4]. Carbon-XANES spectra, shown in Fig. 1, were obtained at four locations on this IDP section, identified as having high C concentrations from the C map. In most areas the spectra showed three pre-edge resonances, though one region (patch 2–4) showed no peaks. The three peaks are π* resonances due to C double or triple bonds. The lowest energy peak can be identified as the C = C double bond. At least two distinct phases of C were identified. The section was thinner than optimal for this technique, so the change in contrast of the C-rich areas across the C edge was only 10%. Even so, individual C-XANES spectra were obtained in ~2 min.

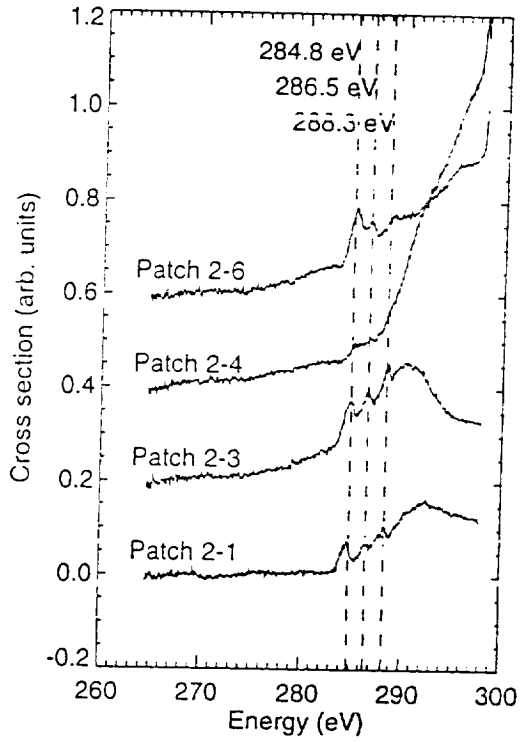

Fig. 1. Carbon-XANES spectra of four regions on a single ultramicrotome section of L2008F4, found by taking the negative of the logarithm of transmission spectra. The spectra have been vertically displaced for clarity.

The STXM can be used to map the C density distribution, determine the C abundance, and identify the particular C bond.

References: [1] Anders E. (1989) *Nature, 342*, 255–257. [2] Flynn G. J. (1993) *LPS XXIV*, 493–494. [3] Jacobsen C. et al. (1991) *Opt. Comm., 86*, 351–364. [4] Ade H. et al. (1994) *Science, 258*, 972–975.

Appendix D:

Arndt, P. and Flynn, G.J. (1995) On the Reliability of PIXE and SXRF Microanalysis of Interplanetary Dust Particles, (abstract) Meteoritics, 30, 482.

ON THE RELIABILITY OF PIXE AND SXRF MICROANALYSES OF INTERPLANETARY DUST PARTICLES. P. Arndt[1] and G. J. Flynn[2], [1]Max-Planck-Institute für Kernphysik, 69029 Heidelberg, Germany, [2]Department of Physics, State University of New York, Plattsburgh NY 12901, USA.

Introduction: The trace-element contents of stratospheric interplanetary dust particles (IDPs) eventually provide clues to their origin(s). Since the masses of IDPs are on the order of nanograms, their trace-element contents typically amount to only about 10^8 atoms. Therefore all analytical techniques are operating near their limits of detection (LODs), and the question is: How reliable are the trace-element data of IDPs?

At present three different analytical techniques are applied to measure trace elements in IDPs: proton-induced X-ray emission (PIXE), synchrotron X-ray fluorescence analysis (SXRF), and time of flight- or double-focusing secondary ion mass spectrometry (TOF-SIMS/SIMS). In 1989 we performed a crosscheck between minor- and trace-element data obtained by SXRF in Hamburg and by PIXE in Heidelberg and found nonconflicting results [1]. Here we report on a new crosscheck between results acquired with the new Heidelberg PIXE facility [2] and the actual SXRF facility in Brookhaven [3].

TABLE 1. Element weight-ppm (assuming Fe = 19.04%)of three IDPs measured with SXRF and PIXE. The errors for SXRF (not yet calculated) are up to 20% on the peaks that are very near the detection limits.

		Ti	V	Cr	Mn	Co
L2005AB2	PIXE	530 ± 30	—	3780 ± 60	3880 ± 90	720 ± 400
	(LOD)	40	50	50	130	690
	SXRF	700	—	3710	3910	—
	(LOD)	—	—	—	—	—
L2011K1	PIXE	350 ± 20	—	1650 ± 40	3650 ± 80	—
	(LOD)	30	70	40	100	690
	SXRF	—	—	—	3800	—
	(LOD)	410	—	—	—	—
L2011R13	PIXE	780 ± 20	61 ± 20	3000 ± 40	1990 ± 50	1330 ±40
	(LOD)	20	40	30	90	650
	SXRF	1080	—	2990	2100	—
	(LOD)	—	—	—	—	—
CI chondrites		436	56.5	2660	1990	502

		Ni	Cu	Zn	Ga	Ge
L2005AB2	PIXE	10130 ± 4	270 ± 20	250 ± 7	10 ± 3	170 ± 6
	(LOD)	10	30	5	7	4
	SXRF	9880	230	210	—	140
	(LOD)	—	—	—	9	—
L2011K1	PIXE	7240 ± 40	195 ± 20	31 ± 4	16 ± 3	26 ± 3
	(LOD)	6	20	6	5	4
	SXRF	7510	140	39	18	25
	(LOD)	—	—	—	—	—
L2011R13	PIXE	15960 ± 5	90 ± 25	361 ± 7	9.2 ± 3	32 ± 3
	(LOD)	20	30	4	5	5
	SXRF	15440	89	340	—	25
	(LOD)	—	—	—	2	—
CI chondrites		11000	136	312	10.0	32.7

		As	Se	Br
L2005AB2	PIXE	—	69 ± 5	42 ± 4
	(LOD)	9	4	2
	SXRF	—	63	48
	(LOD)	5	—	—
L2011K1	PIXE	6.9 ± 3	—	—
	(LOD)	4	10	4
	SXRF	—	—	—
	(LOD)	4	8	7
L2011R13	PIXE	5.9 ± 2	26 ± 3	250 ± 6
	(LOD)	4	4	4
	SXRF	—	17	200
	(LOD)	20	—	—
CI chondrites		1.86	18.6	3.56

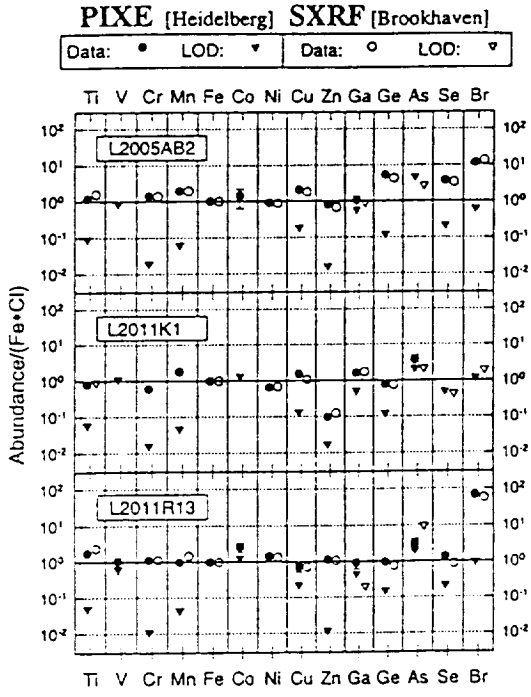

Fig. 1. Elemental abundance ratios in three IDPs as obtained by PIXE (●) and SXRF (○) after normalization to Fe and CI [4]. The respective limits of detection (LODs) are indicated as triangles. The Mn value of particle L2011R13 shown in this figure (2990 ppm) is incorrect because of a typographical error. The correct value is 2100 ppm.

Measurements: Three IDPs, L2005AB2 (≈12 µm), L2011K1 (≈15 × 25 µm), and L2011R13 (≈17 × 34 µm), were first analyzed with SXRF in 1994 and reanalyzed with PIXE in March 1995. The PIXE data were aquired in two runs with different absorbers in front of the detector. One spectrum was obtained with a 45-µm Be absorber and a 5-pA beam of 2 × 2 µm² during 20–50 min for each particle. For a second analysis we used a 155-µm Al absorber and a 5 × 5 µm² beam of ≈300 pA for 60–120 min. The SXRF data were acquired in one run (<30 min) with a thick Al absorber and a beam size of roughly 20 × 20 µm².

Results: The resulting element weight ratios normalized to Fe (set to be ≡19.04% = CI [4]) are presented in Table 1. Abundances normalized to Fe and to the respective CI (=solar) ratios from Anders and Grevesse are shown in Fig. 1. With only a few exceptions, there is a very good agreement between the PIXE and the SXRF results. Since the SXRF data were acquired only with a thick absorber, the SXRF-LODs are rather high (≈CI) for Ti. The largest discrepancy was found in particle L2011R13 for Se (PIXE/SXRF = 1.6). All other elements agree within a maximum factor of 1.4.

Conclusion: PIXE and SXRF analyses of three IDPs (12–30 µm) lead to consistent abundances for the elements from Ti to Br. Thus, major-, minor-, and trace-element data obtained by these two facilities on small particles can be directly compared.

References: [1] Wallenwein R. et al. (1989) *LPS XX*, 1171–1172. [2] Traxel K. et al. (1995) *NIM*, in press. [3] Sutton S. R. and Flynn G. J. (1988) *Proc. LPSC 18th*, 607–614. [4] Anders E. and Grevesse N. (1989) *GCA*, *53*, 197–214.

Appendix E:

Flynn, G.J. (1995) Changes in the Zodiacal Cloud, News and Views in Nature, V. 376, 114.

NEWS AND VIEWS
INTERPLANETARY DUST

Changes in the Zodiacal Cloud

George J. Flynn

AT present about 4×10^7 kg — 40,000 tonnes — of interplanetary dust from the Zodiacal Cloud falls onto the Earth annually[1]. But has this rate been constant through time? Apparently not, according to evidence presented by K. A. Farley on page 153 of this issue[2].

Farley has measured the concentration of ^{3}He solar ions implanted into interplanetary dust, in an oceanic core spanning the period from 0.19 to 69.27 million years ago. After correction for the varying sedimentation rate, Farley finds two maxima in the ^{3}He concentration, occurring 37 and 50 million years ago. He interprets these maxima as periods when dust accretion was a factor of three higher than the mean over the interval from 10 to 20 million years ago, and a factor of six higher than the minimum value (16 million years ago). These results clearly call into question any assumption that, over the past few billion years, the Zodiacal Cloud has been in a steady state, producing a constant interplanetary dust flux at Earth.

Small interplanetary dust particles spiral rapidly into the Sun because of the Poynting–Robertson effect, a process of orbital decay caused by drag from solar radiation. Larger particles become smaller by erosion or catastrophic collisions. It takes under 100,000 years for a typical particle of 10–20 micrometres in diameter, starting at 3 astronomical units out, to spiral into the Sun. So the interplanetary dust presently accreted by the Earth was emitted from much larger objects in the relatively recent past. A constant source of dust, providing about 9×10^3 kg s^{-1}, is required to maintain the Zodiacal Cloud in a steady state[3].

Until recently, comets were believed to be the main source of resupply. But Kresák[4] showed that the total mass of dust emitted by currently active comets provides only 2 per cent of the necessary amount. Whipple[5] proposed that the present Zodiacal Cloud was generated by comet Encke during an early and much more active phase of its evolution, an implicit acceptance that the Zodiacal Cloud is not in steady state. The discovery of dust bands associated with asteroid families[6], and physical evidence from interplanetary dust collected from the Earth's stratosphere[7], suggested that some of the dust comes from asteroids. But analysis of the dust-band data by Dermott *et al.*[8] indicates that main-belt asteroids contribute only 30 per cent at most. In all, the inadequacy of identified dust sources to maintain the Zodiacal Cloud in steady state supports Farley's observation of a time variation in the accretion rate, and further suggests that we are currently in an era of increased dust flux.

This has implications for the sources of the dust. The slowly eroding surfaces of all asteroids and active comets contribute continuously to the interplanetary dust. But from the large peaks in the dust flux, as reported by Farley, it would seem that one, or only a few, dramatic events, such as the catastrophic disruption of a large asteroid or the appearance of an unusually active comet, contribute the bulk of the dust in times of peak intensity.

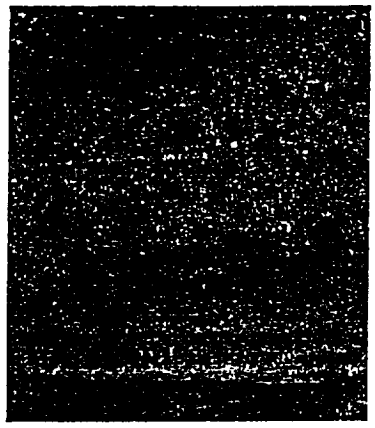

John Sanford/Science Photo Library

'Zodiacal light' seen after sunset as sunlight reflects off zodiacal dust.

During these periods of higher flux, most of the interplanetary dust should reflect the composition and mineralogy of one or a few parent bodies. The abundance of carbon, which is particularly diagnositic of meteorite type and albedo, has been measured in some 60 stratospheric interplanetary dust particles[9,10]. All have carbon contents greater than the carbonaceous chondrite Allende[9,10], suggesting that they do not span the range of albedos, and inferred carbon contents, exhibited by main-belt asteroids[11,12]. Even the most diverse types of interplanetary dust, the hydrated and the anhydrous particles, may originate from a single parent body[13]. This lack of compositional diversity is consistent with the bulk of the interplanetary dust presently falling onto the Earth being derived from one or a few dramatic events[11,12].

An alternative to Farley's interpretation is that these variations record changes in the solar emission rate of ^{3}He, resulting in higher ^{3}He concentrations in dust particles exposed during peaks in the emission. Examination of lunar samples and meteorites shows no evidence that there is much variation in the solar ion flux, although these measurements are not particularly sensitive to short-term variations of a factor of three or so. So the cause of the ^{3}He spikes at 37 and 50 million years ago must be investigated by other techniques.

If, as Farley proposes, ^{3}He has not diffused from its original site and the record is therefore not distorted, intact interplanetary dust from earlier times should be preserved in the core. Farley calculates a concentration of about 7 parts per million of small (up to 50 micrometre) interplanetary dust particles, and up to 700 p.p.m. of larger particles in the sediment that is richest in ^{3}He. These larger particles should be identifiable by mapping sediment sections for elements rich in chondritic particles, followed by chemical and mineralogical studies on the chondritic regions. If Farley is correct, comparison of the 16- and 37-million-year-old layers will show dust concentrations that vary by a factor of six. Furthermore, in the layers recording peaks in the dust flux, the composition and mineralogy of the dust should reflect that of the parent bodies causing the enhancement.

Farley points out that iridium, which is normally used as a tracer of extraterrestrial matter, does not correlate with ^{3}He. This is because iridium traces the total deposition of extraterrestrial material, whereas ^{3}He traces only those extraterrestrial particles that are small enough (less than 50 micrometres) to accumulate a significant bulk concentration of solar ^{3}He and retain that ^{3}He during entry into Earth's atmosphere. Particles smaller than 50 micrometres constitute about 10 per cent of the total mass of interplanetary dust[1], so Farley's results relate directly to only a small fraction of the interpianetary dust falling onto the Earth. Direct identification of dust particles in the sediments would track the flux of particles over the whole size range. □

George J. Flynn is in the Department of Physics, State University of New York at Plattsburgh, Plattsburgh, New York 12901, USA.

1. Love, S. G. & Brownlee, D. E. *Science* **262**, 550–553 (1993).
2. Farley, K. A. *Nature* **376**, 153–156 (1995).
3. Grun, E. *et al. Icarus* **62**, 244–272 (1985).
4. Kresák, L. in *Solid Particles in the Solar System*, IAU Symp. 90 (eds Halliday, I. & McIntosh, J.) 211–222 (Reidel, Dordrecht, 1980).
5. Whipple, F. L. in *Zodiacal Light and the Interplanetary Medium* NASA SP-150 (ed. Weinberg, J. L.) 409–426 (NASA Sci. Tech. Information Office, Washington DC, 1967).
6. Low, F. J. *et al. Astrophys. J.* **278**, L19–L22 (1984).
7. Flynn, G. J. *Icarus* **77**, 287–310 (1989).
8. Dermott, S. F. *et al.* in *Asteroids, Comets and Meteors 1991* (eds Harris, A. W. & Bowell, E.) 153–156 (LPI, Houston, 1992).
9. Schramm, L. S. *et al. Meteoritics* **24**, 99–112 (1989).
10. Thomas, K. L. *et al.* in *Analysis of Interplanetary Dust* AIP Conf. Proc. 310 (eds Zolensky, M. E. *et al.*) 165–172 (American Institute of Physics, New York, 1994).
11. Flynn, G. J. *Meteoritics* **28**, 349 (1993).
12. Flynn, G. J. *Planet. Space Sci.* **42**, 1151–1161 (1994).
13. Zolensky, M. E. & Barrett, R. *Microbeam Anal.* **2**, 191–197 (1993).

Thomas, K.L., Blanford, G.E., Clemett, S.J., Flynn, G.J., Keller, L.P., Klock, W., Maechling, C.R., McKay, D.S., Messenger, S., Nier, A.O., Schlutter, D.J., Sutton, S.R., Warren, J.L., and Zare, R.N. (1995) An Asteroidal Breccia: The anatomy of a Cluster IDP, Geochimica et Cosmochimica Acta, 59, No. 13, 2797-2815.

0016-7037/95 $9.50 + .00

0016-7037(95)00174-3

An asteroidal breccia: The anatomy of a cluster IDP*

K. L. THOMAS,[1] G. E. BLANFORD,[2] S. J. CLEMETT,[3] G. J. FLYNN,[4] L. P. KELLER,[5] W. KLOCK,[6] C. R. MAECHLING,[3] D. S. MCKAY,[7] S. MESSENGER,[8] A. O. NIER,[9] D. J. SCHLUTTER,[9] S. R. SUTTON,[10] J. L. WARREN,[1] and R. N. ZARE[3]

[1]Lockheed, 2400 Nasa Rd. 1, Houston, TX 77058, USA
[2]University of Houston-Clear Lake, Houston, TX 77058, USA
[3]Department of Chemistry, Stanford University, Stanford, CA 94305, USA
[4]Department of Physics, SUNY-Plattsburgh, Plattsburgh, NY 12901, USA
[5]MVA Inc., 5500/Suite 200 Oakbrook Pkwy., Norcross, GA 30093, USA
[6]Institute für Planetologie, Wilhelm-Klemm-Str. 10, 4400 Munster, Germany
[7]NASA/JSC, SN, Houston, TX 77058, USA
[8]McDonnell Center for the Space Sciences, Physics Department, Washington University, St. Louis, MO 63130, USA
[9]School of Physics and Astronomy, University of Minnesota, Minneapolis, MN 55455, USA
[10]Department of Geophysical Sciences, The University of Chicago, Chicago, IL 60637, USA

(*Received April* 22, 1994; *accepted in revised form March* 24, 1995)

Abstract—We report results of a consortium study of a large interplanetary dust particle known as cluster L2008#5. This cluster is composed of fifty-three fragments (>5 μm in diameter) and several hundred fines (<5 μm in diameter). Fragments and some fines were characterized using a variety of chemical and mineralogical techniques including: energy dispersive X-ray analyses for bulk chemical compositions for elements carbon through nickel, transmission electron microscopy for mineralogy, noble gas measurements, synchrotron X-ray fluorescence for trace element abundances, isotopic abundances using an ion probe, trace organic abundances, and reflectance spectroscopy. Our results show that cluster L2008#5 displays strong chemical and mineralogical heterogeneity on a size scale of the individual fragments (~10 μm in diameter). Despite the strong heterogeneity, we believe that nearly all of the analyzed fragments were originally part of the same cluster in space.

Several methods were used to estimate the degree of heating that this cluster experienced. Variations in the inferred peak temperatures experienced by different fragments suggest that a thermal gradient was maintained. The cluster as a whole was not strongly heated; it is estimated to have a low earth-encounter velocity which is consistent with origin from an object in an asteroidal orbit rather than from a comet, which would most likely have a high entry velocity.

Our conclusions show that cluster L2008#5 consists of a chemically and mineralogically diverse mixture of fragments. We believe that cluster L2008#5 represents a heterogeneous breccia and that it was most likely derived from an object in an asteroidal orbit. We also present an important cautionary note for attempts to interpret individual, small-sized 10–15 μm IDPs as representative of parent bodies. It is not unique that individual building blocks of IDPs, such as discrete olivine, pyroxene, sulfide grains, regions of carbonaceous material, and other noncrystalline material, are found in several fragments; however, it is unique that these building blocks are combined in various proportions in related IDPs from one large cluster particle.

INTRODUCTION

Since May of 1981, NASA at the Johnson Space Center (JSC) has used high-flying aircraft to collect interplanetary dust particles (IDPs) in the Earth's stratosphere. The conventional flat plates used for particle collection have a surface area of ~30 cm^2 and capture IDPs, typically with diameters ranging from ~2–25 μm. Within the past five years, large area collectors (LACs), with a tenfold increase in surface area, have also been used to sample the stratospheric particle population. The LACs were found to collect a greater number of larger sized extraterrestrial particles, many with diameters > 25 μm. Although some of these large IDPs remain intact when removed from the collectors, many collide with the collection surface, fracture, and produce fragments of various sizes. We used the term cluster particle for a fragmented, large IDP. In general, a cluster particle is a group of fragments in a clump on a collection surface with a minimum of three large-size fragments (>10 μm in diameter) and many fines (fragments < 5 μm in diameter). The study of cluster particles has several advantages over that of small-sized individual IDPs: (1) cluster IDPs provide a large amount of extraterrestrial material which may be relatively pristine or unheated, (2) fragments from the same cluster can be examined using a variety of techniques, and (3) cluster particles bridge the size-gap from conventional stratospheric IDPs to larger particles. These larger particles, or micrometeorites, generally range from ~100–1000 μm in diameter with a mass distribution peaking near 200 μm (Love and Brownlee, 1993). Extraterrestrial particles in this size range are, by mass, the most abundant material striking the Earth (Grün et al., 1985).

A preliminary mineralogical and chemical study of two to three fragments from several cluster particles showed that, in general, bulk compositions for most major elements were chondritic (within ~2 × CI), with the exception of carbon (Thomas

* This paper is dedicated to the memory of A. O. Nier who greatly contributed to the study of interplanetary dust particles.

Table 1
Bulk compositions of 53 fragments from cluster L2008#5 obtained by quantitative energy dispersive X-ray spectroscopy (EDX).

Fragment	Clu11	Clu13	Clu14	Clu15	Clu16	Clu17	Clu18	Clu19	Clu110	Clu111
Size*	9	15x25	10x20	10	20	10	8x10	10x10	10	12x12
C	14	3	2	2	4	12	4	14	10	6
Na	2.1	0.4	3.1	0.8	1.8	1.7	2.4	1.0	1.6	0.6
Mg	13.3	20.6	6.3	15.6	9.4	11.0	12.2	8.5	9.6	2.7
Al	0.8	0.6	3.1	1.6	1.7	1.2	1.2	1.0	0.9	0.3
Si	10.1	27.7	12.7	22.4	12.4	14.4	14.4	23.8	20.6	6.8
P	0.4	0.0	0.4	0.3	0.4	0.5	0.7	0.7	0.3	0.4
S	4.3	0.2	1.7	0.4	11.2	6.8	4.3	5.6	4.1	25.3
K	0.1	0.7	0.3	1.8	0.0	0.1	0.0	0.0	0.2	0.0
Ca	9.8	0.4	1.6	0.0	1.9	0.8	0.9	0.5	1.0	0.0
Ti	0.0	0.0	0.0	0.0	0.0	0.0	0.0	0.0	0.0	0.0
Cr	0.1	0.5	0.1	0.3	0.1	0.1	0.2	0.1	0.4	0.0
Mn	0.2	0.3	0.1	0.3	0.1	0.1	0.2	0.0	0.2	0.0
Fe	7.9	2.7	28.2	12.7	25.4	16.6	24.2	10.8	19.4	36.9
Ni	0.6	0.0	0.9	0.1	1.6	1.2	0.6	0.6	1.2	3.5
O	36.7	42.6	39.8	41.9	30.1	33.8	34.8	33.2	30.0	17.6
Total**	100.0	99.7	100.3	100.2	100.1	100.3	100.1	99.8	99.5	100.1

Fragment	Clu112	Clu113	Glu114	Glu115	Glu116	Glu117	Glu118	Glu119	Glu120	Glu1121
Size*	10x12	8x10	7x10	8x10	7x10	5x7	8x12	5x5	9x12	10
C	2	7	6	4	2	1	8	6	2	2
Na	1.5	1.0	0.9	1.2	2.2	1.6	0.9	1.6	0.9	1.0
Mg	1.3	17.6	11.3	11.6	9.7	5.1	5.0	8.3	20.4	18.7
Al	0.4	0.7	0.7	1.2	0.9	0.6	1.8	1.0	0.7	0.4
Si	5.6	22.7	11.0	15.4	12.4	10.3	21.5	11.8	26.4	22.3
P	0.4	0.4	0.4	0.3	0.5	0.3	0.4	0.5	0.3	0.2
S	3.9	2.8	13.2	6.7	5.2	7.8	0.5	13.5	0.5	0.2
K	0.0	0.0	0.0	0.0	0.1	0.3	0.3	0.0	0.0	0.0
Ca	0.1	0.2	0.6	1.1	0.9	0.4	13.8	0.6	0.3	0.0
Ti	0.0	0.0	0.0	0.0	0.0	0.0	3.6	0.0	0.0	0.0
Cr	0.9	0.1	0.2	0.2	0.3	0.5	0.0	0.0	0.2	0.3
Mn	0.0	0.1	0.4	0.3	0.3	0.1	0.0	0.1	0.0	0.3
Fe	51.8	6.4	26.8	23.2	30.8	37.6	1.3	25.2	3.5	13.7
Ni	3.4	0.3	1.2	1.3	1.0	2.5	0.0	1.5	0.0	0.0
O	28.2	40.9	27.1	33.5	33.2	31.5	43.0	30.2	44.1	41.2
Total**	99.5	100.2	99.8	100.0	99.5	99.6	100.1	100.3	99.3	100.3

Fragment	Clu21	Clu22	Clu23	Clu24	Clu25	Clu26	Clu27	Clu28
Size*	10x15	8x8	6x9	5x7	5x7	5x5	5x7	5x10
C	4	2	7	5	7	5	8	9
Na	3.2	0.1	1.9	2.7	2.3	1.9	2.6	2.6
Mg	4.4	0.5	9.7	11.8	11.7	11.0	9.1	10.5
Al	0.6	0.1	1.4	1.7	1.5	1.9	4.2	1.4
Si	7.9	0.9	13.3	14.5	15.3	18.4	12.8	14.0
P	0.5	0.2	0.6	0.9	0.6	0.4	0.8	0.6
S	7.1	23.4	9.4	2.8	5.4	6.2	2.0	4.1
K	0.1	0.0	0.1	0.0	0.1	0.3	0.2	0.1
Ca	0.2	0.0	0.5	0.9	0.9	0.1	0.8	0.9
Ti	0.0	0.0	0.0	0.0	0.0	0.0	0.0	0.0
Cr	0.1	0.0	0.3	0.2	0.2	0.2	0.1	0.2
Mn	1.0	0.1	0.1	0.3	0.2	0.1	0.1	0.2
Fe	38.1	57.6	23.4	17.6	18.4	18.8	19.4	19.0
Ni	4.0	0.2	1.5	0.8	1.1	1.8	1.1	1.3
O	29.1	15.2	31.0	40.3	35.6	33.8	39.3	36.3
Total**	100.2	100.4	100.2	99.5	100.3	99.9	100.5	100.2

et al., 1993a). However, the results also indicated that fragments from cluster particles can show chemical and mineralogical heterogeneities at the 10 μm scale which suggests that conclusions drawn from one fragment of a cluster are not necessarily representative of other fragments from the same cluster. These initial results prompted us to do a more systematic investigation of many fragments from one individual cluster particle. Here we report the results of a consortium study in which multiple fragments from one large cluster were distributed to several research groups and analyzed using a variety of mineralogical and chemical techniques. The main objectives of this study were (1) to determine if fragments from a single cluster are chemically and mineralogically heterogeneous, (2) to determine if heterogeneities extend to other properties of cluster IDPs, (3) to compare the chemical and mineralogical properties of a cluster IDP to chondrites, and (4) to compare reflectance spectra of a characterized cluster IDP to those of plausible parent bodies (e.g., asteroids and comets).

METHODS

We were allocated ~95% of the fragments from cluster particle #5 from the large area collector L2008. This cluster contained a mixture of optically light and dark fragments and subfragments, or fines, as observed in reflected light. Based on the number and size of the fragments, without considering pore spaces between individual fragments, we estimate that the original size of this cluster was ~40–50 μm in diameter. It is possible that the cluster is much larger if the porosity is higher (see section "What is the source of cluster

TABLE 1. (Continued)

Fragment	Clu31	Clu32	Clu33	Clu34	Clu35	Clu36	Clu37	Clu38	Clu39	Clu310
Size*	5x5	5x7	5x5	15x17	12x10	8x20	15x15	12x12	12x12	8x10
C	9	17	23	3	2	3	3	3	3	29
Na	2.2	2.4	2.0	0.4	3.0	1.7	1.0	0.5	4.5	1.5
Mg	10.4	9.7	7.1	3.6	9.0	9.6	8.8	2.7	7.0	8.1
Al	1.5	1.1	1.0	0.2	0.8	1.1	0.8	0.2	4.9	1.0
Si	16.4	16.4	16.4	5.8	11.3	12.2	13.1	3.0	19.2	12.3
P	0.5	0.5	0.5	0.2	1.2	0.7	0.1	0.3	3.7	0.5
S	3.4	4.5	6.6	12.4	1.5	9.2	1.0	25.6	1.2	5.9
K	0.1	0.1	0.1	0.0	0.1	0.0	0.0	0.0	0.7	0.1
Ca	1.0	0.6	0.6	0.2	0.7	1.0	1.0	0.0	13.3	0.5
Ti	0.0	0.0	0.0	0.0	0.0	0.0	0.1	0.0	0.0	0.0
Cr	0.2	0.1	0.1	0.2	0.2	0.2	0.3	0.0	0.4	0.1
Mn	0.1	0.1	0.1	0.1	0.4	0.2	0.3	0.0	0.1	0.1
Fe	15.7	13.8	11.6	46.0	34.5	25.5	38.4	47.8	3.7	10.5
Ni	0.7	0.7	0.6	3.0	0.9	2.6	1.8	0.5	0.2	0.6
O	38.5	34.0	30.3	25.0	34.2	32.9	30.2	16.2	37.8	29.8
Total**	100.0	99.9	100.0	100.1	99.8	99.9	99.9	99.8	99.7	99.9

Fragment	Clu311	Clu312	Clu313	Clu314	Clu315	Clu317	Clu318	Clu319	Clu320
Size*	10x10	8x8	8x8	5x12	9	8x10	7x10	8x8	10
C	4	9	15	14	15	2	4	4	12
Na	1.6	1.6	2.2	2.6	2.7	4.5	5.7	1.5	5.4
Mg	7.8	9.0	9.3	9.6	15.5	10.0	7.0	11.1	2.2
Al	0.7	1.4	1.3	1.4	0.9	3.9	10.6	1.2	0.5
Si	10.9	17.5	16.3	14.6	7.4	20.9	13.7	15.1	30.0
P	0.3	0.4	0.5	0.6	0.6	0.3	2.5	0.8	0.5
S	8.2	6.0	4.6	3.7	6.2	0.6	2.4	6.6	0.3
K	0.1	0.1	0.0	0.0	0.0	0.2	0.1	0.0	0.5
Ca	0.8	0.4	0.6	0.6	0.5	0.2	4.0	1.0	0.1
Ti	0.0	0.0	0.0	0.0	0.0	0.0	0.0	0.0	0.0
Cr	0.3	0.2	0.1	0.1	0.0	0.0	0.1	0.3	0.0
Mn	0.2	0.1	0.1	0.0	0.1	0.3	0.1	0.2	0.4
Fe	33.5	18.6	12.5	15.8	12.1	17.9	8.6	20.3	0.9
Ni	1.9	1.1	0.7	0.8	0.3	0.1	0.5	1.2	0.0
O	29.9	34.4	37.1	36.1	38.9	39.4	40.9	36.4	47.1
Total**	100.2	99.8	100.2	99.9	99.9	100.3	100.2	99.7	99.9

Fragment	Clu51	Clu52	Clu53	Clu54	Clu55	Clu56
Size*	10x7	6x6	7x7	10x10	10x10	5x8
C	4	13	5	12	4	4
Na	2.3	1.6	1.8	1.3	2.3	1.3
Mg	9.2	9.6	10.2	10.2	9.4	11.7
Al	0.8	2.0	1.0	1.0	1.8	1.2
Si	13.3	18.3	15.7	16.5	16.0	17.4
P	0.6	0.7	0.6	0.5	0.5	0.6
S	10.6	5.0	7.0	9.4	5.8	9.4
K	0.0	0.1	0.0	0.0	0.0	0.0
Ca	1.0	2.2	0.9	0.8	0.5	0.9
Ti	0.0	0.0	0.0	0.0	0.0	0.0
Cr	0.1	0.1	0.3	0.2	0.1	0.3
Mn	0.1	1.0	0.2	0.2	0.2	0.2
Fe	23.1	11.3	26.1	17.1	19.4	16.4
Ni	2.3	0.6	1.2	0.8	4.3	0.9
O	32.3	35.1	29.9	30.5	36.1	35.3
Total**	99.7	100.6	99.9	100.5	100.4	99.6

*Size in micrometers
**Totals may not equal 100.0; C abundances are reported as whole number values

L2008#5?''). Fragments include three that are ~15 × 15 μm, six that are ~12 × 12 μm, ~50 that range from 5–10 μm in diameter, and several hundred subfragments (also called fines) < 5 μm in diameter. The fifty-three fragments (>5 μm in diameter) from cluster L2008#5 were placed on beryllium substrates for analysis at JSC using a JEOL 35 CF scanning electron microscope (SEM) operated at 15 kV and equipped with a Princeton Gamma Tech (PGT) X-ray energy dispersive (EDX) spectrometer. The PGT spectrometer is a detector with a thin organic window which was used to determine bulk particle compositions; this spectrometer allows detection of elements with $Z > 5$. Our complete procedures and analytical checks for quantitative SEM EDX light element analysis of IDPs are described in detail elsewhere (Thomas et al., 1993b).

Following the initial bulk chemical analyses at JSC, multiple fragments were distributed to several research groups for the following analyses: mineralogical studies using transmission electron microscopy (TEM), noble gas measurements, trace element abundances by Synchrotron X-ray Fluorescence (SXRF), ion microprobe studies for isotopic compositions, microprobe two-step laser mass spectrometer (μL^2MS) for trace organic chemistry, and reflectance spectroscopy using a microscope photometer (Fig. 1).

TEM

Ten of the fragments and ten of the fines were embedded in epoxy, thin sectioned using an ultramicrotome, and examined with a JEOL

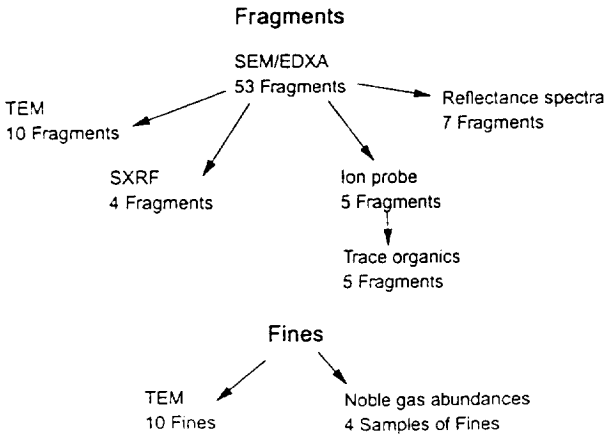

FIG. 1. Methods flowchart showing the types of analyses performed on fragments and fines from cluster L2008#5.

2000 FX TEM equipped with a Link EDX spectrometer. Modal mineralogy was determined for fragments and fines as described in Klöck et al. (1989).

Noble Gas Measurements

Helium content and the helium release temperatures for four samples were determined by step-heating experiments (technique described in detail by Nier and Schlutter, 1993). Each sample consisted of several fines, which approximate a fragment 10 μm in diameter. The fines, which were folded into a square of tantalum foil called an oven, were heated, the gas was extracted, and helium measurements were made by a mass spectrometer.

SXRF

This technique, which is particularly sensitive for the elements from chromium to bromine, was used to determine trace element abundances in four large fragments. The analytical method is described in detail by Flynn and Sutton (1991).

Ion Probe

The Washington University modified IMS-3f microprobe was used to determine hydrogen, carbon, and nitrogen isotopes of eight fragments. A primary ion beam of 8.5 KeV Cs^+ ions was used to analyze the fragments. Hydrogen, carbon, and nitrogen (measured as CN) were measured as negative secondary ions. Carbon and nitrogen isotopic measurements were performed at a mass resolving power of 5,500 and hydrogen isotopic measurements were performed at low mass resolution. Further details of the technique can be found in McKeegan et al. (1985).

Trace Organic Composition

Following ion probe analysis, the same fragments were analyzed for the presence of polycyclic aromatic hydrocarbons (PAHs). PAHs signatures were obtained with a μL^2MS (Kovalenko et al., 1992; Clemett et al., 1993).

Reflectance Spectra

Spectra over the visible wavelength range (380–800 nm) were acquired for seven fragments using techniques described by Bradley et al. (1994).

RESULTS AND DISCUSSION

Chemistry and Mineralogy

Table 1 shows normalized element abundances for fifty-three fragments analyzed from cluster L2008#5; ~25% of the fragments contain at least one major element with non-chondritic abundances. Table 2 shows the mean, standard deviation, and range of element abundances of all fragments. The cluster mean for all elements is chondritic, within a factor of two of CI, with the exception of minor elements sodium, phosphorus, and titanium which were ~4 × CI, ~5 × CI, and 2.5 × CI, respectively. The range of major elements (C, O, Mg, Si, S, and Fe) and the cluster mean are shown graphically in Fig. 2; large ranges for major elements suggest that compositional differences exist (also see Table 1). Chemical heterogeneity of individual

Table 2
Mean composition (wt.%) and range of element abundances of 53 fragments from cluster L2008#5. Bulk composition of Orgueil (CI) is shown for comparison.

	Cluster Fragments Mean and 1σ Variations (Wt.%)	Range	Bulk Composition of Orgueil (CI)* (Wt.%)
C	7 ± 3.7	1-29	3.5
O	34.0 ± 2.3	15.2-47.1	46.4
Na	1.9 ± 0.6	0.1-5.7	0.5
Mg	9.5 ± 0.9	0.5-20.6	9.5
Al	1.4 ± 0.2	0.1-10.6	0.9
Si	14.9 ± 0.7	0.9-30.0	10.7
P	0.6 ± 0.1	0.0-3.7	0.1
S	6.3 ± 4.2	0.2-25.6	5.3
K	0.1 ± 0.1	0.0-1.8	0.1
Ca	1.4 ± 0.1	0.0-13.8	0.9
Ti	0.1 ± 0.0	0.0-3.6	0.04
Cr	0.2 ± 0.1	0.0-0.9	0.3
Mn	0.2 ± 0.1	0.0-1.0	0.2
Fe	21.1 ± 0.5	0.9-57.6	18.5
Ni	1.2 ± 0.1	0.0-3.5	1.1

*Normalized without water, Anders and Grevesse (1989)

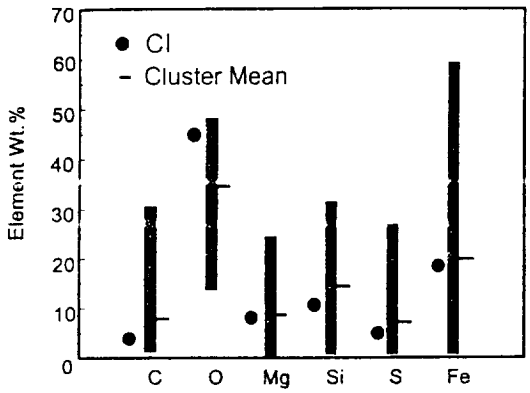

FIG. 2. Range and mean of major element abundances for fifty-three fragments from cluster L2008#5. Average values are also shown for Orgueil (CI). The range of element abundances varies widely among fragments; however, the cluster mean is chondritic (within 2 × CI).

cluster fragments is shown in a Si-Mg-Fe (atomic) triangular plot (Fig. 3). Individual fragments display a variety of compositions ranging from Si- to Fe-rich. More than 50% of the fragments plot in the region between the solid-solution tie lines for pyroxene and olivine; this region also represents solar abundances for these elements. Atomic Mg/(Mg + Fe) values range from 0.2–0.95 with the cluster average at 0.51 (Fig. 4).

Representative bulk EDX analyses of eighteen fragments are shown in Table 3. Fragments are grouped according to their chemical compositions; e.g., some fragments are clearly dominated by sulfides, magnetite, or carbonaceous material, while others have a bulk chondritic composition. In general, fragments dominated by sulfides have lower oxygen abundances, and sulfur and iron are > 2 × CI. In two fragments, Clu111 and Clu34, Ni is > 2 × CI suggesting that kamacite or Ni-rich iron sulfide (e.g., pentlandite) could be present. In the magnetite-dominated chemical group, sulfur abundance ranges from 1.0–7.8 wt% and Fe > 2 × CI. Of the representative fragments with chondritic element abundances, Clu51 has Ni > 2 × CI and S ~ 2 × CI; this fragment contains Ni-rich and Ni-poor iron sulfides. Mineralogy was determined for two of the chondritic fragments: Clu18 is composed primarily of fine-grained aggregates containing ~10 nm Fe metal and Fe-sulfide grains embedded in a silica-rich glassy matrix, while Clu51 contains a mixture of olivine and pyroxene grains (also see Table 3). Of the fifty-three fragments analyzed, twelve were carbon-rich fragments with C > 3 × CI (~11 wt%). All other major element abundances are within 2 × CI for the C-rich fragments.

For comparison to other published data, we have normalized some of our element abundances to silicon; the atomic abundance ratios to silicon for IDPs and other extraterrestrial materials are shown in Table 4. The average ratios of major elements are essentially the same for the cluster fragments, anhydrous IDPs, and 10–20 μm fragments of the Orgueil CI chondrite, with the exception of carbon. Although the heterogeneity is the same for cluster IDPs and other fine grained chondritic material (e.g., chondrite matrix), the grain size in IDPs is, in general, much finer than the grain size of chondrites. Some coarse (5–10 μm) fragments from both L2008#5 and Orgueil are nonchondritic (e.g., individual fragments are dominated by single minerals such as olivine, iron sulfides, etc.) unlike the fine-grained anhydrous IDPs, which have chondritic compositions.

Tables 5 and 6 list mineral assemblages found in ten large fragments and fines from cluster L2008#5. Fragments have been classified according to the most abundant mineral phase. A variety of mineral phases are present in this cluster particle, and minerals with similar compositional ranges are found in

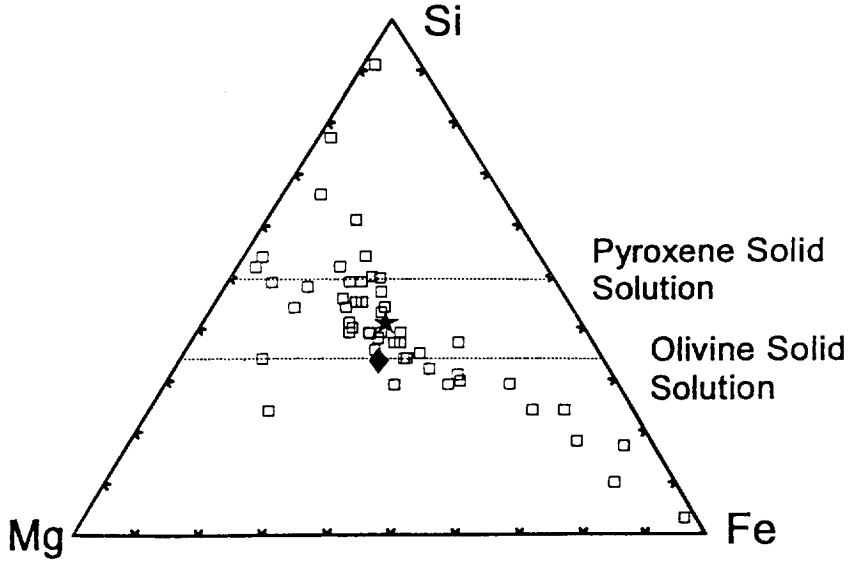

FIG. 3. Atomic abundances of Si-Mg-Fe for fifty-three cluster fragments are shown on a triangular plot. Fragments range in composition from Si- to Fe-rich. The cluster average is located between the olivine and pyroxene compositional tie lines indicating that L2008#5 is composed of a subequal mixture of olivine and pyroxene. The value for CI plots close to that for the cluster average. Key: □, cluster fragments; ★, cluster average; ♦, Orgueil (CI).

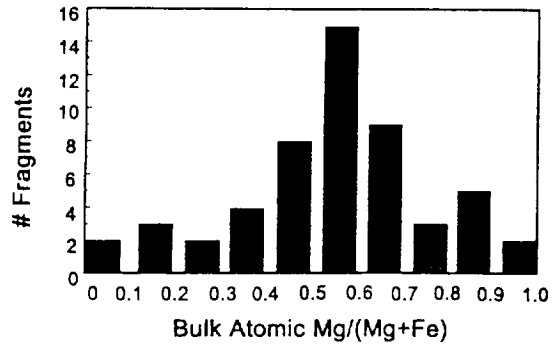

FIG. 4. Atomic Mg/(Mg + Fe) values for fifty-three fragments range from 0.2–1.0 with an average at 0.51. The mean value for Orgueil (CI) is 0.55.

large fragments and fines. For example, olivine compositions range from Fo 57–99 in large fragments and from Fo 66–98 in fines. However, several olivine-dominated fragments have ranges of olivine compositions which differ from one fragment to another (e.g., Clu35 and Clu317). Some fragments contain olivines with narrow ranges, or equilibrated compositions (e.g., Clu51 and Clu52, Fig. 5a) and others have olivines with large ranges, or unequilibrated compositions (e.g., Clu35 and Clu17, Fig. 5b).

Pyroxene compositions include enstatite and high-Ca pyroxenes. Low-Fe, Mn-enriched (LIME) silicate grains were observed in two fragments and one fine. Silicates with this unique composition have been previously reported from some anhydrous IDPs and chondritic meteorite matrices (Klöck et al., 1989). Fine-grained aggregates (FGAs), also known as unequilibrated aggregates (Bradley, 1994a), tar balls (Bradley and Brownlee, 1988), and GEMS (glass with embedded metal and sulfides; Bradley, 1994b) are the major constituents in two fragments (Clu52 and Clu17); they are observed as minor components in one fragment (Clu11) and two fines (#2 and #7). All FGAs in fragments and fines from L2008#5 are composed of a glassy matrix with embedded metal and sulfides. Fe-sulfides with Ni (FSN) are present in most fragments and fines.

Noncrystalline regions, typically <500 nm in size, composed of carbonaceous material or glass are present in some fragments. We observed amorphous, carbonaceous material in four fragments with C > 3 × CI. Carbonaceous material can have a smooth or vesicular texture (Fig. 6a,b); we did not observe carbonaceous material in the fines. Noncrystalline, noncarbonaceous solids have compositions which range from Si-rich to feldspathic with minor amounts of magnesium and iron present in some regions; some glassy regions contain considerable iron, up to 25 wt%. Glassy areas have either a smooth or a vesicular texture. Mineral grain sizes vary from fragment to fragment: of the twenty fragments and fines examined, nine have constituent grains that are predominantly coarse grained (~1 μm in diameter) (e.g., fragment Clu317, Fig. 7a), six are predominantly fine grained (<50 nm in diameter) (e.g., fragment Clu17, Fig. 7b), and five contain a mixture of coarse and fine grains. Partial magnetite rims were observed in fourteen of twenty fragments and fines from this cluster (e.g., fragment Clu17, Fig. 8).

Noble Gas Measurements

Helium content and helium release temperatures for four samples were determined by step-heating experiments. The four samples are fines estimated to make up a 10-μm sized fragment. The average ^{4}He abundance is ~4.1 (cc × 10^{11}) and the extraction temperatures for removal of 50% of the He range from 750–1040°C, with an average at 928°C (Table 7). In previous work on twenty individual IDPs, the average ^{4}He abundance was 4.6 (cc × 10^{11}) (Nier and Schlutter, 1992) which is close to the cluster average (Table 7). However, the range of ^{4}He is from ~0 (undetectable) to 17. The average ^{4}He abundance of 24 IDPs from unrelated, cluster IDPs is 4.7 (cc × 10^{11}) and the range is from 0.33 to 44.6 (Table 7, Nier and Schlutter, 1993). The 50% helium release temperature for these IDPs is 798°C. The average ^{4}He abundance is nearly identical for individual IDPs, unrelated cluster IDPs, and cluster L2008#5 fragments, indicating that the exposure history is similar for all three groups of IDPs. The range of ^{3}He/^{4}He exhibited by the individual and unrelated cluster IDPs is much larger than that of the L2008#5 cluster fragments, possibly due to the small number of fragments analyzed. The average 50% He release temperature for the cluster fragments is significantly higher than that of unrelated cluster IDPs (928 vs. 798°C, respectively) suggesting that this cluster was heated, on average, to higher temperatures during atmospheric entry. Helium release temperatures observed from our four cluster fragments are significantly different (750°C vs. a group ranging from 910–1040°C). The low helium release temperature of one fragment suggests that it was not strongly heated during atmospheric entry while the high release temperatures of three others suggest they were strongly heated; the range of fragment temperatures indicates that this cluster has likely maintained a thermal gradient during atmospheric entry, especially if the cluster was very porous and if it contained components subject to sublimation (e.g., organic material, water).

^{3}He/^{4}He ratios are given for three groups of IDPs, bulk carbonaceous and unequilibrated ordinary chondrites, and four samples of Nogoya (Table 7). The ^{3}He/^{4}He range for cluster L2008#5 is 3.3–7.2 (×10^4), which is within that for both groups of IDPs, as well as bulk CM, and CV chondrites.

SXRF

Four fragments from L2008#5 were analyzed by SXRF to determine trace element abundances. With the exception of zinc in one IDP, the individual fragments show variations of individual element abundances essentially spanning the entire range of individual analyses reported by Flynn et al. (1993) for all anhydrous IDPs. All fragments show deviations by more than a factor of two from CI for at least three elements (Fig. 9 and Table 8). The only consistent trends are enrichments in copper, selenium, and bromine, and a depletion in zinc relative to CI.

Two fragments show marked depletions in zinc (Zn/Fe < 0.1); Zn/Fe ratios range from 0.2–0.5 for the remaining fragments (Table 8). With the exception of the zinc depletion, which is seen in all fragments, there is no obvious pattern

Table 3
Representative analyses of sulfide-dominated, magnetite-dominated, chondritic, and carbon-rich fragments from cluster L2008#5. (Minor elements are excluded resulting in low totals).

Representative bulk analyses of sulfide-dominated fragments

Element Wt%	Clu38	Clu111	Clu22	Clu34
C	3	6	2	3
O	16.2	17.6	15.2	25.0
Mg	2.7	2.7	0.5	3.6
Si	3.0	6.8	0.9	5.8
S	25.6	25.3	23.4	12.4
Fe	47.8	36.9	57.6	46.0
Ni	0.5	3.5	0.2	3.0
Total	98.8	98.8	98.0	98.8

Representative bulk analyses of magnetite-dominated fragments

Element Wt%	Clu21	Glu117	Clu112	Clu37
C	4	1	2	3
O	29.1	31.5	28.2	30.2
Mg	4.4	5.1	1.3	8.8
Si	7.9	10.3	5.6	13.1
S	7.1	7.8	3.9	1.0
Fe	38.1	37.6	51.8	38.4
Ni	4.0	2.5	3.4	1.8
Total	94.6	95.8	96.2	96.3

Representative bulk analyses of chondritic fragments

Element Wt.%	Clu25	Clu24	Clu18	Clu28	Clu51	Clu116
C	7	5	4	9	4	2
O	35.6	40.3	34.8	36.3	32.3	33.2
Mg	11.7	11.8	12.2	10.5	9.2	9.7
Si	15.3	14.5	14.4	14.0	13.3	12.4
S	5.4	2.8	4.3	4.1	10.6	5.2
Fe	18.4	17.6	24.2	19.0	23.1	30.8
Ni	1.1	0.8	0.6	1.3	2.3	1.0
Total	94.5	92.8	94.5	94.2	94.8	94.3

Representative bulk analyses of carbon-rich fragments

Element Wt.%	Clu310	Clu313	Clu32	Clu33
C	29	15	17	23
O	29.8	37.1	34.0	30.3
Mg	8.1	9.3	8.7	7.1
Si	12.3	16.3	16.4	16.4
S	5.9	4.6	4.5	6.6
Fe	10.5	12.5	11.6	11.6
Ni	0.6	0.7	0.6	0.6
Total	96.2	95.5	92.8	95.6

suggesting genetic links between the fragments. Flynn and Sutton (1991) have previously reported the analyses of two stratospheric particles which were recovered from the collectors intact but which broke into several fragments before trace element analysis. One of these (L2003E1) separated into three fragments. All elements from chromium to selenium were within a factor of three of CI except Cr (4.5 × CI) in one fragment and selenium (0.17 × CI) in another fragment. Each fragment exhibited a similar bromine enrichment. These fragments of L2003E1 showed a much narrower range of variation in element abundances than did the fragments of cluster L2008#5. The second fragmented IDP (U2015G1) (Sutton and Flynn, 1988) exhibited significant compositional heterogeneity with Ni/Fe differing by a factor of three and the Zn/Fe differing by a factor of nine between the two fragments.

The zinc content of individual IDPs correlates well with other indicators of severe heating (Flynn et al., 1992; Keller et al., 1992; Thomas et al., 1992). Zinc is depleted relative to CI in all four fragments with two showing the very low Zn/Fe ratios suggestive of significant heating. The range of Zn/Fe ratios of Clu16 and Clu18 is an order of magnitude lower than that for fragments Clu21 and Clu319 indicating different degrees of heating between the pairs of fragments, assuming comparable initial zinc levels.

Despite the heterogeneity between fragments of this cluster, the average composition of the four fragments agrees well with the average previously reported by Flynn et al. (1993) for eight heated, anhydrous IDPs (Table 8, Fig. 10). The average composition of the cluster fragments shows the general enrichment of volatile elements relative to CI meteorites which is characteristic of smaller, individual IDPs (Flynn et al., 1992), with depletions in zinc and germanium consistent with significant heating (Flynn et al., 1994).

Isotopic Measurements

Ion microprobe measurements of hydrogen isotopes were performed on five fragments with a range of bulk carbon

Table 4
Comparison of atomic abundance ratios to silicon (ranges in parentheses) for cluster fragments, anhydrous IDPs, and other extraterrestrial materials

	L2008#5 Fragments[a]	Anhydrous IDPs[b]	Anhydrous IDPs[c]	Orgueil Fragments[b]	Orgueil[d]	CM Matrix[e]	CV Matrix[e]	UOC[f]	Comet Halley[g]
C	1.1	2.0	2.4	0.6	0.8				4.4
	(0.2-4.6)	(0.7-4.9)		(0.0-1.3)					
O	4.0	4.0	4.0	5.1	7.6				4.8
Na	0.2	0.1	0.05	0.09	0.05	0.04	0.02	0.12	0.05
Mg	0.7	0.8	1.0	1.0	1.0	1.0	1.0	0.5	0.5
	(0.04-1.6)	(0.5-1.8)	(0.6-2.0)	(0.04-1.2)					
Al	0.1	0.1	0.07	0.1	0.08	0.1	0.1	0.12	0.04
S	0.4	0.4	0.4	0.2	0.4	0.2	0.05	0.05	0.4
	(0.01-1.5)	(0.2-1.3)	(0.1-1.8)	(0.01-0.5)					
Ca	0.07	0.04	0.05	0.1	0.06	0.03	0.07	0.02	0.04
Cr	0.008	0.008		0.008	0.02	0.01	0.01		
Mn	0.008	0.008		0.004	0.01	0.006	0.006		
Fe	0.7	0.6	0.7	0.73	0.87	0.89	0.93	0.6	0.3
	(0.03-1.9)	(0.2-2.0)	(0.2-2.0)	(0.02-2.1)					
Ni	0.04	0.02	0.02	0.06	0.05	0.06	0.04	0.03	0.02

[a] This work.
[b] Thomas *et al.* (1993b).
[c] Schramm *et al.* (1989).
[d] Anders and Grevesse (1989).
[e] McSween and Richardson (1977). (CM, CV).
[f] Huss *et al.* (1981). (Semarkona).
[g] Jessberger *et al.* (1988).

abundances (Table 9). Three of the fragments were subsequently measured for carbon and nitrogen isotopes as well. Four C-poor fragments were obtained by crushing Clu37, which was previously determined to contain 3 wt% C. Subsequent EDX analysis confirmed that all subfragments had low carbon abundances. Four C-rich (10–29 wt%) fragments were analyzed as well. These included Clu110, Clu313, and two subfragments of Clu19, and nine subfragments of Clu310.

Deuterium enrichments (δD) were observed in three of the four C-rich fragments and range from +322 to +822 ‰ (Table 9). Three of the four C-rich fragments were also found to have ^{15}N enrichments of up to 260 ‰. No substantial carbon isotopic anomalies were observed.

Trace Organic Chemistry

Four fragments were analyzed for trace organic components using microprobe two-step mass spectrometry (μL^{2}MS) (Kovalenko et al., 1992). These fragments had been analyzed previously for D/H isotopic ratios using the ion microprobe technique described in the previous section. In the first step of μL^{2}MS, constituent molecules of the sample are desorbed with a pulsed infrared laser beam which is focused to microscopic dimensions. For this study, either a CO_2 laser (λ = 10.6 μm) or Nd:YAG laser (λ = 1.064 μm) was used, giving a spatial resolution of ~40 μm or ~5 μm, respectively. The choice of desorption laser is determined by the particle size and proximity of other fragments on the sample mount. Both lasers give similar mass spectra; the difference is the spatial profile. The laser power is kept low enough (~10^6 W/cm^2) to ensure desorption of neutral organic species with little or no fragmentation. In the second step, polycyclic aromatic hydrocarbons (PAHs) in the desorbed plume are preferentially ionized by a pulsed ultraviolet laser beam (Nd:YAG, λ = 266 nm) which passes through the plume. The wavelength provides selectivity through resonance enhanced multiphoton ionization according to mass.

PAHs were observed in several of the cluster fragments, most notably Clu19(β) and Clu110 (Table 9). Significant variability of the PAH signature was observed both among different fragment particles and among subfragments of the same particles. The variation in signal is partially correlated, as would be expected, to the size of the fragment, however there are clear exceptions. For example, a strong distribution of aromatic species was observed in Clu19(β) (Fig. 11), whereas no signal was observed in Clu19(α) above the detection limits of the instrument,† each fragment having approximately the same dimensions. The mass spectra of PAHs from those fragments show evidence of aromatic species which are very different from those of two previously studied unrelated IDPs, Aurelian (U47-M1-2a) and Florianus (U47-M1-7a) (Clemett et al., 1993). Both the mass range of aromatic species observed and the structural complexity are reduced, ranging primarily from one to six fused ring species with little indication of alkylation (replacement of -H with -$(CH_2)n$CH$_3$, where n = 0, 1, 2···). However, individual peak intensities in some cases (e.g., naphthalene and chyr-

† The detection sensitivity for a given PAH species depends both on its concentration in the sample and its photoionization cross section (Zenobi and Zare, 1991). The ultimate detection sensitivity for the molecule coronene (C_{24}, H_{12}, 300 amu) has been measured in the μL^{2}MS instrument to be 0.8 attomoles (~500,000 molecules in a 40 μm analysis spot), and that for the molecule phrenanthrene (C_{14}, H_{10}, 178 amu) ~0.02 attomoles (~12,000 molecules in a 40 μm analysis spot).

Table 5
Mineralogy of ten large fragments from cluster L2008#5

Fragment	Olivine	Enstatite	Pyroxene (Hi Ca)	FGA*	FSN**	C-type Material	Glass	Others	Mineral Grain Sizes (CG†, FG‡)	Mt Rim•
Olivine-Dominated										
Clu317	Fo 63-68; 1Fo 95				Rare	Not Obsv. 2 wt.%	Yes		CG	Yes
Clu11	Fo 79-84	Yes	Yes	Rare	Yes	Obsv. 14 wt.%			CG & FG	Yes
Clu35	Fo 57-82	Yes			Rare	Not Obsv. 2 wt.%	Yes	Chromite	CG & FG	Yes
Pyroxene-Dominated										
Clu13	1 Fo 88	~99%			Yes	Not Obsv. 3 wt.%		Kamacite	CG & FG	Yes
Clu315		Yes			Yes	Obsv. 15 wt.%		Fe Metal, Kamacite	FG	No
Olivine-Pyroxene Mix										
Clu51	Fo 84	Yes				Not Obsv. 4 wt.%	Yes		FG	Yes
FGA Dominated										
Clu52	Fo 95; LIME••	Yes; LIME••		Yes	Yes	Obsv. 13 wt.%			FG	No
Clu17	Fo 79-99	Yes		Yes	Yes	Obsv. 12 wt.%	Yes		FG	Yes
Others										
Clu38	Rare, Fo 65-76				Large, single	Not Obsv. 3 wt.%			CG	Yes
Clu318		LIME••			Rare	Not Obsv. 4 wt.%	Yes	Large Mag-netite	CG	Yes

*Fine grain aggregate **Fe-Sulfide with Ni †Coarse-grained ‡Fine-grained •Magnetite Rim
••LIME Low iron, manganese-enriched (From Klöck *et al.*,1990).

sene/triphenylene) are more intense than the most intense peaks observed previously from Aurelian.[‡] Additionally, spectra are dominated by even mass PAHs with little evidence of odd mass peaks observed in Aurelian and Florianus. The odd mass peaks were previously interpreted as nitrogen containing functional groups such as -CN or $-NH_2$ attached to an aromatic chromophore. It is likely that the distribution of PAHs observed in Clu19 and Clu110 may have been perturbed by prior exposure to the ion probe (10 KeV Cs^+ ions) used for the D/H measurements; however, as observed previously by Clemett et al. (1993), strong PAHs signals are only observed in deuterium-rich particles (also see Table 9). Deuterium enrichment alone does not necessarily indicate that PAHs will be present, but PAHs signals have only been observed on deuterium-rich particles. PAHs and elemental carbon coexist in some fragments of this cluster; however, considering the mass of the entire cluster, they appear to be inhomogeneously distributed.

[‡] Care must be taken in comparing different mass peak intensities since ion intensities are not only proportional to the concentration of the compound in the sample, but also the photoionization adsorption cross section for that compound at the laser ionization wavelength (λ = 266 nm).

Reflectance Spectra

Visible wavelength reflectance spectra were acquired from seven individual fragments from cluster L2008#5 (Fig. 12). Fragments were randomly selected for maximum variability; some are chondritic while others are dominated by single mineral grains. All spectra show a rise into the red, similar to that in certain primitive asteroids, although two fragments (Clu33 and Clu313) exhibit a slight decline at ~800 nm. These two fragments are the most C-rich of the seven IDPs (Table 10). Reflectivity values range from 3–18% (Table 10 and Fig. 12). Two fragments with the highest albedos, Clu39 and Clu111, are dominated by large single mineral grains (Ca-rich pyroxene and Fe-Ni sulfide, respectively). Five fragments have albedos which are essentially indistinguishable:

Table 6
Mineralogy of ten fines from cluster L2008#5

Sample	Olivine	Enstatite	Pyroxene (Hi Ca)	FGA*	FSN**	C-type Material	Glass	Others	Mineral Grain Sizes (CG†, FG‡)	Mt Rim•
Olivine-Dominated										
1	Fo 78						Yes	Chromite	CG	Yes
2	Fo 85	Yes; 1 LIME••		Yes			Yes	Kamacite	CG & FG	Yes
3	Fo 86	Yes	Yes		Yes		Yes	Magnetite	CG	Yes
Pyroxene-Dominated										
4		Yes	Yes						CG	Yes
5			Yes		Yes				FG	Yes
Olivine-Pyroxene Mix										
6	Fo 66	Yes			Yes		Yes		CG & FG	Yes
FGA Dominated										
7	Fo 98		Yes	Yes	Yes				FG	No
Others										
8	Fo 68-91				Yes			Lg. Magnetite	CG	No
9					Yes			Lg Magnetite & Kamacite	CG	No
10		Yes			Yes		Yes	Kamacite Chromite Ferrihydrite	CG	No

*Fine grain aggregate **Fe-Sulfide with Ni †Coarse-grained ‡Fine-grained •Magnetite rim
••LIME Low iron, manganese-enriched (From Klöck *et al.*, 1990).

Clu313, Clu33, Clu23, Clu37, and Clu111 (Fig. 12). The bulk carbon abundance ranges from 3–23 wt% for these five fragments. Although the two C-rich fragments (Clu33 and Clu313) have low albedos, other fragments which have chondritic carbon abundances exhibit nearly identical albedos (Clu37 and Clu23). Clu37 is probably dominated by magnetite; this fragment has 38.4 wt% Fe and ~1 wt% S (Table 3). Clu23 is chondritic for all major elements although sulfur is approaching 2 × CI abundance, suggesting iron sulfides are present. Fragment Clu312 has the lowest albedo and has chondritic abundances for all elements. Our data suggest that several criteria (carbon content, chemical, and mineral abundances) influence albedos and slopes of reflectance spectra.

The average reflectance spectrum for the seven fragments of L2008#5 is shown in Fig. 13a. The reflectance (~8% at 550 nm) and spectrum shape are comparable to spectra from several carbonaceous chondrites (5–10%; e.g., Hiroi et al., 1993). Reflectance spectra for "typical" S, M, C, P, and D asteroids are shown in Fig. 13b (Zellner et al., 1985). The average spectrum for the seven fragments shows differences from the spectra of common asteroids. The average cluster spectrum has a lower albedo and lacks the reddened slope of S-type asteroids, and is significantly brighter than the P- and D-type spectra; however, analyzed fragments were selected based on their diverse bulk chemical abundances which emphasizes interfragment variations of albedos.

DISCUSSION AND IMPLICATIONS

In the following sections we discuss and summarize some of the more important observations associated with cluster particle L2008#5: (1) the types of carbonaceous materials, including bulk carbon, carbon and nitrogen isotopes, PAHs, and the coexistence of these carbonaceous phases within a fragment, (2) the interfragment variability of carbonaceous materials, (3) cluster heating during atmospheric entry, (4) possible sources for this cluster based on our estimations of size, porosity, entry velocities, and reflectance spectra, and (5) our hypothesis that this cluster is a breccia based on the physical and chemical variations between fragments.

Carbonaceous Phases

Bulk carbon abundances

Carbon abundance ranges from 2–29 wt% (see Tables 1, 2, and Fig. 2). The cluster average is 7 wt% C which falls within the range exhibited by CI chondrites. Carbonaceous material is observed in TEM thin sections of fragments with

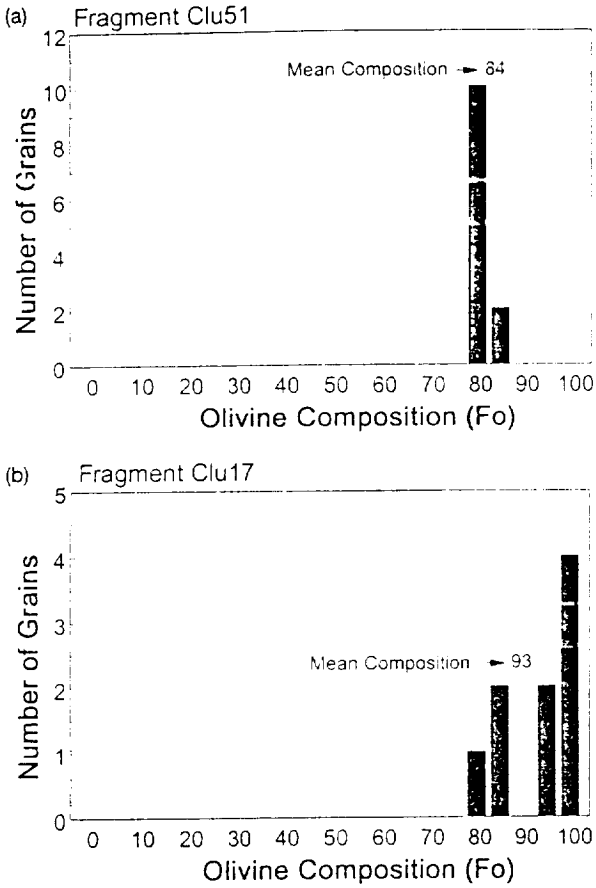

FIG. 5. Olivine compositions in two fragments from cluster L2008#5. (a) Fragment Clu51 contains olivines with equilibrated compositions which range from ~Fo 80–85 with an average at ~Fo 84. (b) Fragment Clu17 contains olivines with unequilibrated compositions; olivines range from ~Fo 80–100 with an average at Fo 93.

C > 3 × CI. The C-rich material is amorphous or poorly crystalline and in some instances exhibits vesicular textures. The amorphous carbon material is not distributed equally among fragments (see Table 5, carbonaceous material). For example, coarse-grained fragments tend to be C-poor (<5 wt% C), while those rich in FGAs have high carbon contents (~12 wt% C). However, amorphous carbonaceous material is still rather evenly distributed in C-rich fragments; it acts as a matrix holding individual grains together (Figs. 6a,b, and 14).

Isotopic and PAH measurements

We investigated the chemical state of the carbon in fragments with bulk carbon abundances ranging from 3–29 wt% by two complementary techniques: ion microprobe measurements of hydrogen, carbon, and nitrogen isotopes of each fragment and μL^2MS measurements which are exceptionally sensitive to the presence of PAHs.

We found substantial D enrichments in most of the C-rich fragments analyzed with enrichments ranging from +322 to +822‰. The apparent correlation of D enrichments with carbon content supports the assertion by McKeegan et al. (1985, 1987) that the D-rich carrier phase in IDPs is organic and not water of hydration. This degree of D enrichment appears to be too great to be caused by known solar system processes (Geiss and Reeves, 1981). The enrichment is commonly considered to be due to the partial retention of much larger enrichments of precursor molecules which formed in a presolar molecular cloud from ion-molecule chemistry.

Since the isotopic measurements were made on bulk samples, and μL^2MS measurements may reflect a relatively small fraction of the total organic matter present, it is not possible to identify the isotopic analyses with the PAHs observed in a given particle. However, to date, strong PAH signals have

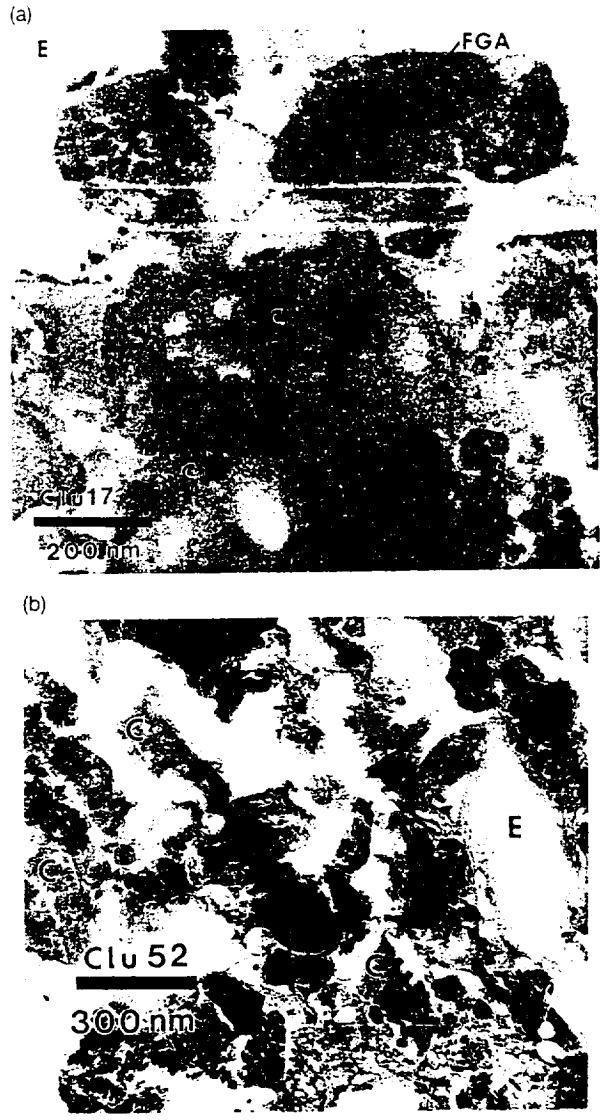

FIG. 6. TEM photomicrographs of thin sections of two fragments from cluster L2008#5. (a) Carbonaceous material (C) in fragment Clu17 has a vesicular texture. This fragment contains fine grain aggregates (FGAs); epoxy (E) is used as the embedding medium. (b) A lower magnification TEM image of carbonaceous material in fragment Clu52. The texture of the carbonaceous regions is vesicular which suggests that another phase, possibly polycyclic aromatic hydrocarbons (PAHs), was lost due to heating during atmospheric entry.

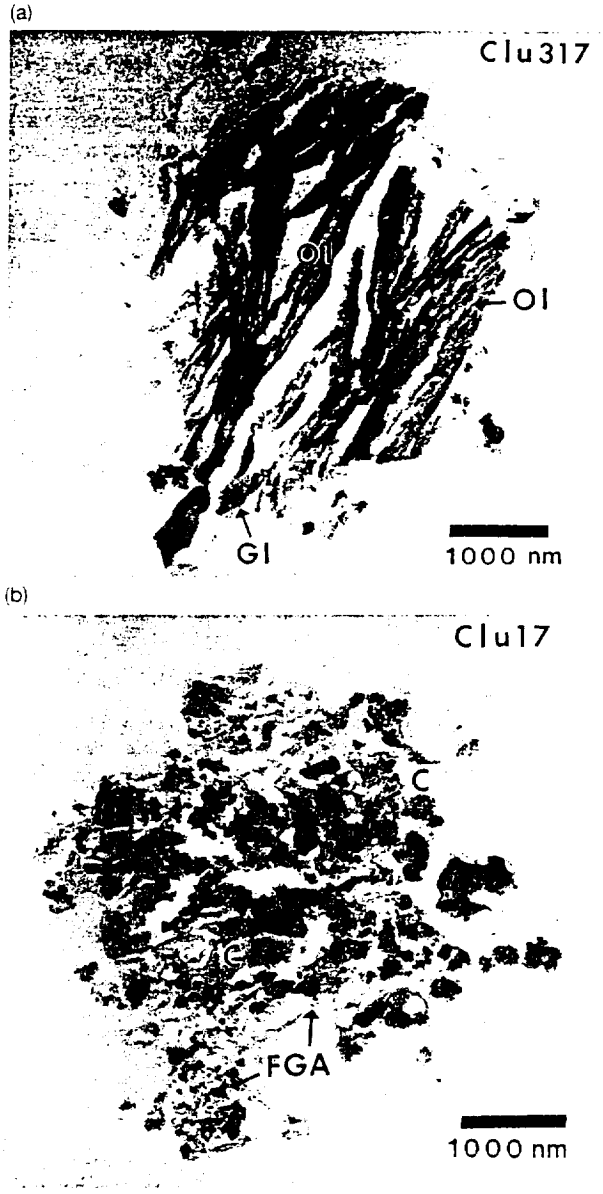

FIG. 7. Low magnification TEM photomicrographs of thin sections of two fragments from L2008#5. (a) Fragment Clu317 is coarse-grained and composed mainly of olivines and glass; light gray areas of epoxy surround the fragment thin section. (b) Fragment Clu17 has a fine-grained, primitive texture and contains mainly carbonaceous material, pyroxene, iron sulfides, and fine-grain aggregates (FGAs).

only been observed in deuterium-rich particles (Clemett et al., 1993; this work). Deuterium enrichments have been observed in every class of organic molecules that has been analyzed in Murchison including PAHs (Pizzarello et al., 1991; Krishnamurthy et al., 1992; Cronin et al., 1993).

We also found substantial ^{15}N enrichments in both fragments yielding strong PAH signals (Table 9). ^{15}N enrichments are expected to result from low temperature ion-molecule chemistry, but to a much smaller degree than the observed D enrichments (Adams and Smith, 1981). Substantial ^{15}N enrichments have been previously observed in IDPs (Stadermann et al., 1989), and a number of primitive meteorites (Kerridge 1985; Ash et al., 1993). Although the precise carrier phase(s) is not well constrained, ^{15}N enrichments appear to be associated with organic matter (Ash et al., 1993). It is interesting to note that two of the three IDPs observed to have strong PAH signals also carry ^{15}N enrichments (Clemett et al., 1993), though as in the case of the D enrichments, more work will be required to establish possible links of isotopic anomalies with PAHs in IDPs.

PAHs appear to be distributed heterogeneously throughout the cluster and do not seem to be correlated with any particular phase, although there is a rough correlation with size for those fragments showing evidence of PAHs. The mass distribution of PAHs is unique and has not been observed previously by μL^2MS on either chondritic meteorites or IDPs. We observed vesicular textures in the carbonaceous regions of some fragments of this cluster that were not analyzed individually by μL^2MS; this texture has been observed previously in other C-rich IDPs (Thomas et al., 1993b, 1994). A vesicular texture may be a consequence of evaporative loss of low-mass PAHs during a heating event; the heating event probably includes atmospheric entry and/or by ion bombardment during isotope analysis in the case of Clu19 and Clu110. Atmospheric entry heating is anticipated to effect PAHs in three ways: (1) they may be volatilized possibly recondensing on other fragments, (2) they may be fragmented with only some of the organic molecules being volatilized, or (3) they may undergo free-radical polymerization leading to involatile complex higher molecular weight species (Lewis, 1979; Greinke and Lewis, 1984). Since some of the cluster fragments contain PAHs with masses ranging from 400–500 amu, which are higher than the aromatic structures observed by μL^2MS in both ordinary and carbonaceous chondrites, these may be either compounds unique to IDPs or the product of the polymerization of lower molecular weight species. In the latter case, the PAH distributions may provide clues as to the degree of thermal processing experienced by an IDP during atmospheric entry.

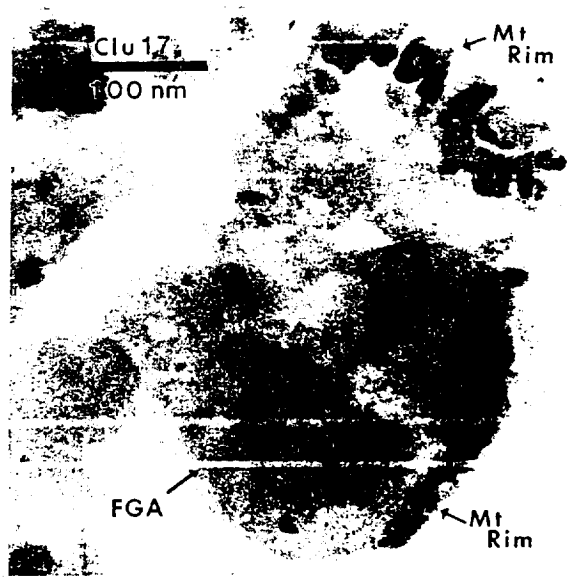

FIG. 8. Partial magnetite rim, <50 nm thick, on an edge of a fine-grained region of fragment Clu17.

Analysis of acid residues for PAHs in seventeen ordinary and carbonaceous chondrites (Clemett et al., 1992) shows that there are notable differences in both the distribution of parent PAHs and the degree of alkylation between the chondrite classes. This is interpreted to be a consequence of secondary processing such as thermal metamorphism and/or aqueous alteration on the original PAH distribution. Over fifty different molecular species have been detected in the chondritic residues, and none have masses significantly larger than 300 amu. This predominantly low-mass distribution is different from the cluster fragments which have PAHs with masses greater than 400 amu.

Heating Summary of Cluster Fragments

Four criteria were used to determine the extent to which L2008#5 was heated during atmospheric entry: (1) the presence of magnetite rims, (2) helium content and helium release temperatures, (3) SXRF trace element abundances, and (4) bulk sulfur content. Magnetite rims form on the exposed surfaces of grains located on the perimeter of the particle during entry into the Earth's atmosphere (Keller et al., 1992). We have observed partial, discontinuous magnetite rims on most cluster fragments and fines. However, we did not find magnetite rims on every fragment or fine. The TEM results suggest that (1) the cluster particle was uniformly heated and only developed magnetite on its exposed surfaces resulting in a diffusional gradient or (2) a thermal gradient was maintained by the cluster such that only the exterior surfaces were strongly affected during entry heating. The variability of helium release temperatures supports the latter interpretation in that most fragments contain little helium and have correspondingly high release temperatures, although one fragment has a release temperature that is significantly lower than the majority. The low abundances of some volatile trace elements (e.g., zinc) also suggest that some fragments have been strongly heated (as indicated by a major depletion in zinc) while other fragments retain chondritic levels of zinc. Seven fragments, with chondritic abundances for other major elements, show depletions in bulk sulfur (Table 1). If these frag-

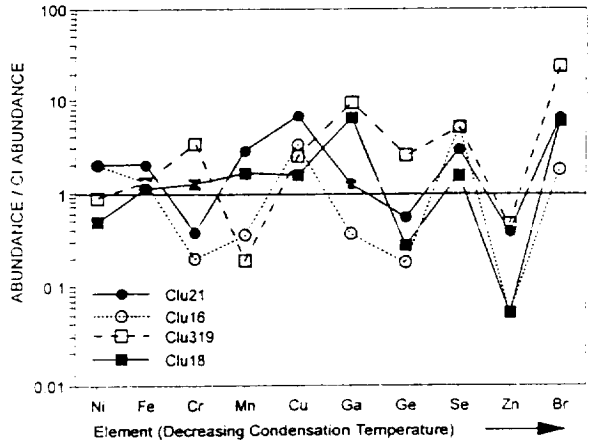

FIG. 9. Average CI normalized trace element abundances in four cluster fragments. Elements are ordered with decreasing nebula condensation temperature. Although element abundances show variation among fragments, some trends are apparent such as enrichments in copper, selenium, and bromine and depletions in zinc.

Table 7
He measurements of fines from cluster L2008#5 and other extraterrestrial materials

Sample	^{4}He (cc x10^{11})	50% He Release Temp. (°C)	^{3}He/^{4}He (x10^4)
IDPs			
1	4.5	750	3.3 +/- 0.7
2	6.1	1040	4.7 +/- 0.5
3	3.4	1010	7.2 +/- 1.2
4	2.2	910	5.9 +/- 1.4
Average	4.1	928	
Average of 20 individual IDPs*	4.6		
Range*	~0-17		1.9-6.4
Average of 24 unrelated cluster IDPs**	4.7	798	
Range**	0.33-44.6	550-1020	2.6-200
Meteorites			
Bulk Orgueil and Ivuna (CI)†			1.4-5.8
Bulk Murray, Mighei, Nogoya (CM)†			1.7-34.1
Bulk Ornans and Kainsaz (CO)†			109-154
Bulk Vigarano, Mokoia, Allende (CV)†			1.5-18.7
Nogoya (CM), 4 samples‡			1.7-3.4
Unequilibrated Ordinary Chondrites†			66-231

* Nier and Schlutter (1992)
** Nier and Schlutter (1993)
†Schultz and Kruse (1989)
‡Black (1972)

ments are assumed to have originally contained chondritic abundances of sulfur, then they have experienced sufficient heating during atmospheric entry to drive off some of the sulfur. Although theoretical models would predict that thermal gradients in particles < 100 μm in diameter are difficult to achieve and maintain, recent calculations suggest that endothermic reactions have a significant effect in moderating heat transfer from the particle surface to the core (Flynn, 1995). If so, then, we may be seeing evidence of a thermal gradient in an anhydrous IDP.

What is the Source of Cluster L2008#5?

Although the relative proportion of cometary and asteroidal dust entering the Earth's atmosphere has not been established, it is widely believed that near-Earth gravitational enhancement favors collection of IDPs that are of asteroidal origin (Flynn, 1990, 1994). Brownlee et al. (1993) suggest that up to 80% of IDPs which range in size from 5–15 μm in diameter originate from asteroidal bodies while the remaining ~20% are derived from objects in cometary orbits. In order to determine possible sources for this cluster, we need to calculate possible entry velocities; if the velocity value is less than or equal to 15 km/s, then it is more likely that the cluster is of asteroidal origin (Flynn, 1989). Although we do not know the original size of the parent particle for cluster L2008#5, we can put reasonable limits on its prefragmentation size in order to estimate the potential entry velocity. Here let us consider three models to constrain the pre-entry size, porosity, and density of L2008#5. We make the following assumptions for Model 1 (Fig. 15): (1) there is essentially no porosity between fragments and intrafragment porosity is low so the original size of the cluster is based on summing the volumes of individual fragments: this assumption leads to the estimate that the cluster would be ~40–50 μm in diameter assuming a spherical shape; (2) the initial density was ~2 g/cm^3 based on the mineralogy and observed porosity in microtome thin sections of the fragments; and (3) the cluster survived passage through the stratosphere without being heated to more than 1350°C, the approximate temperature at which chondritic material would melt and ablate (Love and Brownlee, 1994); we did not observe partial melting of any mineral grains in any fragments of L2008#5. Using the assumptions for Model 1, a cluster IDP 40–50 μm in diameter would yield peak Earth

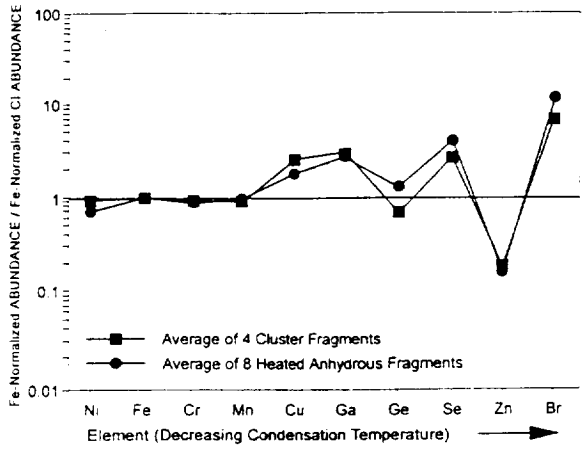

FIG. 10. Comparison of Fe-normalized element abundance/Fe-normalized CI abundance of the average of four cluster fragments and eight heated, anhydrous IDPs (from Flynn et al., 1993). The plots are nearly identical for all elements for both groups of IDPs.

encounter velocities of 15–16 km/s according to thermal models for atmospheric entry heating (e.g., Love and Brownlee, 1994). This velocity range is consistent with an asteroidal or cometary origin for this cluster; it includes velocities for asteroidal particles and the lowest possible velocity for cometary particles. Model 1 places an upper limit on the entry velocity because no interfragment porosity was considered and the highest possible entry temperature was used. However, the cluster probably had a certain degree of porosity because it fractured (along weak junctions between fragments) into many fragments and fines on the collection surface.

In Model 2, we use more reasonable estimates of entry temperature, porosity, and density consistent with the mineralogical data. A better estimate of entry temperature would be from observations of magnetite formed on fragment surfaces and the 50% helium release temperature. Magnetite rims were found on many fragments and fines; they are generally thought to be formed over a range of temperatures, on the order of ~600–1000°C. The 50% helium release temperature may be a truer estimate of the peak temperature experienced during atmospheric entry of small particles (Brownlee et al., 1995). The highest 50% helium release temperature for this

Table 8
SXRF trace element abundances normalized to CI of 4 large fragments from cluster L2008#5 compared with abundances from 8 individual, heated IDPs.

Sample	Cr	Mn	Fe*	Ni	Cu	Zn	Ga	Ge	Se	Br	Zn/Fe
Clu16	0.2	0.4	1.4	2.0	3.5	0.06	0.4	0.2	6.1	2.0	**0.04**
Clu18	1.3	1.8	1.3	0.5	1.7	0.06	7.1	0.3	1.8	7.3	**0.05**
Clu21	0.4	3.1	2.1	2.0	7.4	0.44	1.4	0.6	3.4	7.3	**0.2**
Clu319	3.5	0.2	1.1	0.9	2.6	0.52	10.0	2.8	5.4	24.8	**0.5**
Fragment Average	1.4	1.4	1.5	1.4	3.8	0.3	4.7	1.0	4.2	10.4	**0.2**
Average of 8 Anhydrous IDPs**	0.8	1.0	1.0†	0.8	1.9	0.2	3.0	1.3	4.2	12.4	**0.2**

*Values from EDS
†Fe-normalized
**Flynn *et al.* (1993)

Table 9
Bulk carbon abundance (Wt.%), Deuterium (δD), ^{13}C enrichments, ^{15}N enrichments, and the presence of PAHs signatures in several large fragments from cluster L2008#5. Deuterium abundances are also given for bulk carbonaceous and unequilibrated chondrites.

Sample	C (Wt.%)	δD (per mil)*	$\delta^{13}C$ (per mil)	$\delta^{15}N$ (per mil)	μL^2MS **
IDPs					
Clu310(α)•	29	+89 ± 77			<5
Clu310(β)•	29	+56 ± 83			<5
Clu310(χ)•	29	+71 ± 75	-4 ± 7	+89 ± 27	<5
Clu310(δ)•	29	+66 ± 75	-8 ± 7	+56 ± 33	<5
Clu310(ε)•	29	+17 ± 79	-32 ± 9	+61 ± 32	<5
Clu310(ϕ)•	29	-14 ± 72			<5
Clu310(γ)•	29	-35 ± 6	-16 ± 13	+125 ± 36	<5
Clu310(η)•	29	-55 ± 18	-22 ± 27	+136 ± 38	<5
Clu310(ι)•	29	+44 ± 27			<5
Clu313†	15	+322 ± 67			Not Measured
Clu19(α)‡	14	+664 ± 84	-16 ± 26	+260 ± 34	<5
Clu19(β)‡	14	+424 ± 71	-33 ± 5	+202 ± 16	100
Clu110	10	+822 ± 91	-18 ± 10	+180 ± 18	43
Clu37(α)§	3	-24 ± 17			20
Clu37(β)§	3	+25 ± 22			7
Clu37(χ)§	3	-14 ± 36			32
Clu37(δ)§	3	+12 ± 29			13
Meteorites					
Bulk Carbonaceous Chondrites (CI)•		+44 to +300			
Bulk Carbonaceous Chondrites (CM)•		-176 to +990			
Bulk Carbonaceous Chondrites (CO)•		-116 to +2150			
Bulk Carbonaceous Chondrites (CV)•		-77 to +440			
Bulk Unequilibrated Ordinary Chondrites••		-77 to +3109			

* Terrestrial range is -200 to +50 per mil
** Integrated signal intensity from 80-450 amu normalized relative to Clu19 (β) = 100
• Clu310 broke into 9 separate pieces (α, β, χ, δ, ε, ϕ, γ, η, ι); analyzed by YAG desorption laser
†3 μm fragment too small for PAHs analysis
‡ Clu19 broke into 2 separate pieces (α & β)
§ Clu37 fractured into 4 pieces (α, β, χ, δ)
•Kerridge (1985)
••McNaughton *et al.* (1981)

cluster is 1040°C (Table 7), and considering the errors associated with the measurement, we are using 1100°C as the maximum entry temperature for Model 2. We previously assumed that our original cluster was 50 μm in diameter and had a density of 2 g/cm^3 with essentially no porosity (Fig. 15). Although fragments from this cluster display a range of porosities (i.e., coarse- and fine-grained fragments have widely divergent porosities), they average ~50%. This porosity is consistent with values estimated for other chondritic porous IDPs (e.g., Flynn and Sutton, 1990), although there are reports of IDPs with much lower densities (~0.1 g/cm^3, Rietmeijer, 1993; ~0.3 g/cm^3, Love et al., 1994). For Model 2, our estimate of density is ~1 g/cm^3 based on the same mass as used in Model 1 but incorporating the 50% porosity estimate. With these assumptions, the estimated prefragmentation diameter would be 63 μm (Fig. 15). Further increases in the estimated porosity result in lower densities. For example, a cluster with a porosity of 75% has a density of 0.5 g/cm^3 and a diameter of ~80 μm. In Model 2, assuming the peak temperature is 1100°C, then the entry velocity of the cluster is < 14 km/s, which is consistent with an asteroidal origin (see Love and Brownlee 1994; a 30 μm particle with a density of 2 g/cm^3 is treated the same as a particle 60 μm in diameter with a density of 1 g/cm^3). A cluster with a density 0.5 g/cm^3 and ~80 μm in diameter would have an entry velocity < 13 km/s. In fact, as the density decreases and the size of the cluster increases, the probability rises that this cluster is from an asteroidal source. Previous results from Love and Brownlee (1991) imply that virtually all of the unmelted micrometeorites > 70 μm in diameter are asteroidal in origin, considering there is no contribution from low velocity comets. We agree with others (e.g., Brownlee et al., 1995) that the 50% helium release temperature may vary with the presence of differing mineral phases and particle porosity so it cannot be precisely related to the peak temperature reached during atmospheric entry; however, our best estimate of size, density, entry temperature, and velocity for this cluster suggest that L2008#5 is very likely an asteroidal IDP.

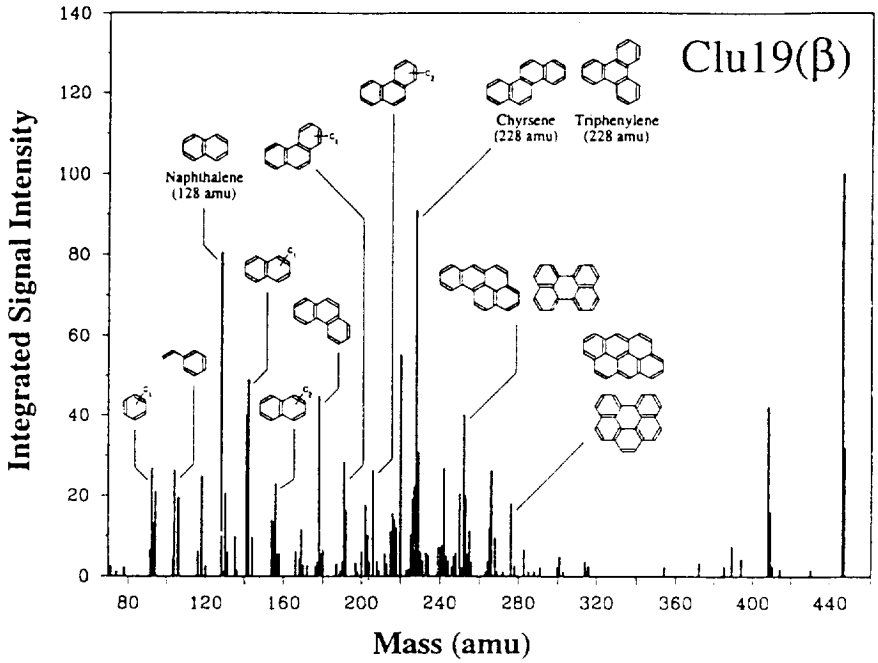

FIG. 11. The μL^2MS spectrum of the cluster particle Clu19(β), for the purposes of display, the signal intensities have been integrated over the mass range of $-1/2$ to $+1/2$ amu for each mass unit and the resulting data plotted as a histogram. The spectrum was generated from thirty single shot time-of-flight spectra (mass resolution ~ 1500), where each single-shot spectrum was stored in a computer, and later calibrated and co-added. Spectra assignments of a few of the more prominent parent PAH species and their alkylated homologs have been indicated. No peaks higher than 450 amu were observed.

Is Cluster L2008#5 a Breccia?

Our data on cluster L2008#5 show that it is clearly heterogeneous on a scale of 10–15 μm, the scale represented by the individual analyzed fragments. This heterogeneity includes both mineralogy and chemistry. While about 25% of the fragments are clearly dominated by a single large mineral grain such as iron sulfides or magnetite, most fragments consist of fine-grained material. Much of the heterogeneity results from differences from region to region within the cluster of the relative abundances of fine-grained mineral, glass, and carbonaceous material. For example, some fragments are rich in fine-grained olivine or pyroxene, others are rich in carbonaceous material, and others are rich in FGAs. If we did not know that these fragments came from the same cluster, we would probably consider that the fragments came from totally different parent sources.

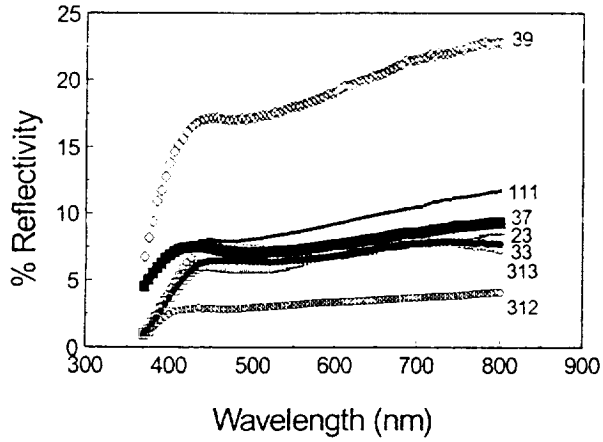

FIG. 12. Reflectance spectra over the visible wavelength range (380–800 nm) of seven fragments from cluster L2008#5. All spectra show a rise into the red; the albedos range from 3–23%. Fragment Clu39, which has the highest albedo, is composed mainly of a single clinopyroxene grain. Fragment Clu312, with the darkest albedo, has a chondritic composition for all major elements including carbon. Fragments Clu111, Clu37, Clu23, Clu33, and Clu313 do not have significantly different albedos although the carbon content is highly variable. For example, bulk carbon is ~3 wt% in Clu37, ~15 wt% in Clu313, and ~23 wt% in Clu33.

Earlier we showed that chondritic fragments have markedly different mineralogies. Chondritic fragments are dominated by olivines, by pyroxenes, by FGAs, or by a mixture of olivine and pyroxene grains (Tables 5 and 6). Furthermore, within a fragment, the olivines may be mostly unequilibrated showing

Table 10
Reflectivity (%) and bulk carbon abundance of seven fragments from cluster L2008#5

Fragment	% Reflectivity (at 575 nm)	C (Wt.%)
Clu312	3	9
Clu313	6	15
Clu33	6	23
Clu23	6.5	7
Clu37	7	3
Clu111	8	6
Clu39	18	3

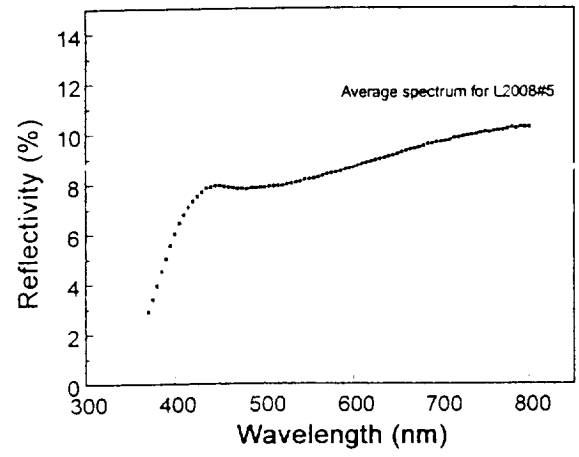

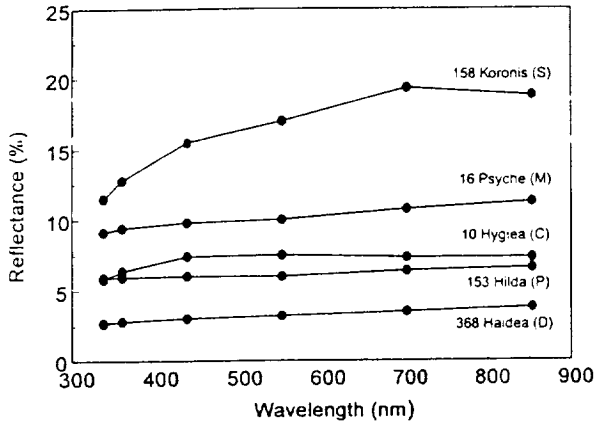

FIG. 13. Comparison of reflectance spectra for cluster L2008#5 and "typical" asteroids. (a) The average reflectance spectrum for seven fragments from cluster L2008#5. (b) Spectra for typical C-, D-, M-, P-, and S- type asteroids. S-type asteroids have reddened slopes and P- and D-type spectra are significantly darker than the average cluster spectrum (ECAS data from Zellner et al., 1985; Albedos from Tedesco, 1989).

a wide range of compositions or, by contrast, may have a narrow range of equilibrated compositions. Olivines from fine-grained fragments with "primitive textures," such as Clu17, have unequilibrated compositions which range from ~Fo 80–100 (Fig. 5b). In general, these fine-grained fragments are predominantly composed of pyroxene, FGAs, and carbonaceous material (Figs. 6a,b, and 7b). Clu51 is an example of a fragment with a coarse-grained texture; it contains equilibrated olivines with mean compositions of ~Fo 84 (Fig. 5a). *The presence of some fragments with fine-grained textures and unequilibrated mineralogies and other fragments with coarse-grained textures and equilibrated mineralogies suggests that cluster L2008#5 is really a breccia containing a physical mixture of material which has had significantly different histories.*

We consider three plausible mechanisms which can produce the heterogeneity we observe in fragments of L2008#5: (1) mixing of IDPs on the collection surface, (2) mixing of diverse mineral grains in the solar nebula, or (3) combining different lithologies from an asteroidal parent body (McKay et al., 1989). First, there is a possibility that the chemical and

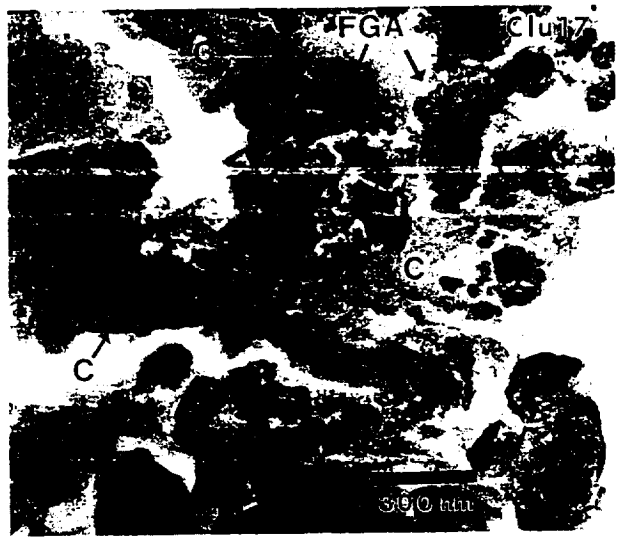

FIG. 14. Fine-grain aggregates (FGAs) embedded in carbonaceous material (C). This texture is typical of carbon-rich fragments in cluster L2008#5 and other fine-grained anhydrous IDPs with C abundance > 3 × CI (Thomas et al., 1994).

mineralogical heterogeneities observed in L2008#5 could be the result of multiple impacts of different IDPs on the same location of the collection surface. However, we believe that all of the fragments are related to the same cluster because (1) the mineralogical and textural heterogeneity of the large fragments is duplicated in the fines, (2) the observed degree of heterogeneity is comparable to that observed in other cluster particles (Thomas et al., 1993a), and (3) the L2008 col-

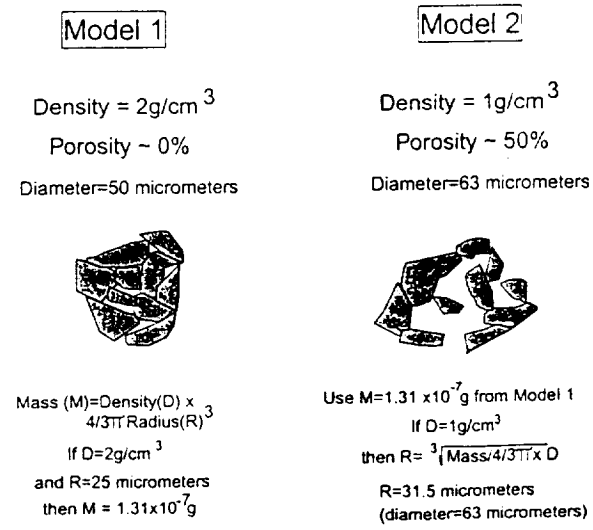

FIG. 15. Cartoon showing the effect of density upon size of a cluster particle. The particle has an assumed spherical shape (Volume = $4/3\pi R^3$). In Model 1, the mass is calculated for a particle having a diameter of 50 μm, density = 2 g/cm^3, and essentially no porosity (Mass = Volume × Density); this is our first estimation of cluster size. In Model 2, the mass calculated in Model 1 is used to determine the size of a particle with a density of 1 g/cm^3 and a porosity of 50%; a diameter of 63 μm is calculated for a cluster particle with the stated characteristics.

lection surface contained a low loading of IDPs and little background material, such as ash or aerosol particles. The fragments associated with L2008#5 were estimated to cover a surface area of ~100 μm^2 on the collector. According to recent work by Flynn (1994), assuming a specific particle density on the collector, the surface area covered by this cluster could have been impacted with, at most, one contaminant fragment ~5 μm or less in diameter.[5] If true, this contaminant fragment would constitute a very small proportion of the cluster. We conclude that essentially all of the analyzed fragments were originally part of the same large cluster.

We have shown that cluster L2008#5 exhibits fine scale heterogeneities in most of its chemical and mineralogical properties; we are left to speculate whether the heterogeneity in this cluster is a reflection of nebular or parent body processing. The fine-scale heterogeneity may have been generated during dust accretion in the early solar nebula. Thus, diverse mineral grains and carbonaceous materials were mixed, accreted, and little changed from that point forward. Alternatively, the heterogeneity may have resulted by mixing of different lithologies on an asteroidal parent body. These differences provide information on the potential parent body for the cluster and may indicate from which region within the parent body the cluster was derived. The cluster particle is anhydrous, and so it apparently escaped the effects of aqueous alteration. In addition, the cluster, in its entirety, has not equilibrated (e.g., magnesium abundances of olivines and pyroxenes are still highly variable; see Fig. 4), thus precluding any significant post-accretional thermal metamorphism on its parent body.

In previous work, Thomas et al. (1993b) analyzed ~20 individual, small-sized IDPs, placed them into three groups based on their mineralogy, and speculated on sources for these particles. They suggested that the anhydrous pyroxene-dominated, C-rich IDPs originated from cometary rather than asteroidal sources because of their high bulk carbon abundance and the fine-grained pyroxene which are unlike any from chondrite matrix. They also suggested that the low-carbon, olivine-dominated anhydrous IDPs may be derived from anhydrous asteroids. In the present study, we have found both types of IDP material, those that are pyroxene-dominated and rich in carbon and those that are olivine-dominated and carbon poor, existing in one cluster particle. Are previous implications for IDP sources now incorrect? The prior study of small-sized IDPs provides a wealth of information on individual fragments, but without additional information to constrain entry velocities (e.g., noble gas measurements), identification of source parent bodies can be ambiguous (e.g., asteroidal or cometary). However, cluster particles present a unique opportunity to study inter-fragment relationships that can only be determined as we examine larger-sized IDPs.

CONCLUSIONS

1) Cluster L2008#5 displays a remarkable chemical and mineralogical heterogeneity on a size scale of the individual fragments which we analyzed (10–15 μm). The mineralogy and chemistry of the individual fragments span a wide range of previously analyzed anhydrous particles.
2) Despite this remarkable heterogeneity, there is strong evidence that nearly all of the analyzed fragments were originally part of the same ~50 μm diameter cluster in space.
3) The low Earth-encounter velocity estimated for this particle (<14 km/s) is consistent with origin from an object in an asteroidal orbit.
4) This cluster is essentially a heterogeneous breccia made up of materials having different histories which were physically combined either in the early nebula or in the regolith of a parent body. We infer that the source region of this asteroid is a complex mixture of fragments and clasts from diverse sources having diverse histories; the resulting breccia represented by cluster L2008#5 has provided us with a rich sampling of many different products.
5) Heating during atmospheric entry has occurred and is quite variable, showing that thermal equilibrium was not attained. However, these heating effects can be unraveled using previously documented characteristics such as the formation of magnetite rims, helium measurements, and depletion of zinc.
6) These results on cluster L2008#5 provide an important cautionary note for attempts to interpret individual 10–15 μm IDPs as representative of parent bodies.

[5] These calculations were done using measurements of particle surface densities of small area collectors from Zolensky and MacKinnon (1985). Surface density measurements may be different on large area collectors but have not yet been determined.

Acknowledgments—Constructive reviews of this manuscript were provided by John Bradley, two anonymous reviewers, and Sue Wentworth. This work was supported in part by NASA RTOPs 152-17-40-23 and 199-52-11-02.

Editorial handling: G. Crozaz

REFERENCES

Adams N. G. and Smith D. (1981) $^{14}N/^{15}N$ Isotope fractionation in the reaction $N_2H^+ + N_2$: Interstellar significance. *Astrophys. J. Lett.* **247**, L123.

Anders E. and Grevesse N. (1989) Abundance of the elements: Meteoritic and solar. *Geochim. Cosmochim. Acta* **53**, 197–214.

Ash R. D., Morse A. D., and Pillinger C. T. (1993) The survival of presolar organic material in CR chondrites? *Meteoritics* **28**, 318–319 (abstr.).

Black D. C. (1972) On the origins of trapped helium, neon, and argon isotopic variations in meteorites-II. Carbonaceous meteorites. *Geochim. Cosmochim. Acta* **36**, 377–394.

Bradley J. P. (1994a) Nanometer-scale mineralogy and petrography of anhydrous interplanetary dust particles. *Geochim. Cosmochim. Acta* **58**, 2123–2134.

Bradley J. P. (1994b) Chemically anomalous, preaccretionally irradiated grains in interplanetary dust from comets. *Science* **265**, 925–929.

Bradley J. P. and Brownlee D. E. (1988) Analysis of chondritic interplanetary dust thin sections. *Geochim. Cosmochim. Acta* **52**, 899–900.

Bradley J. P., Brownlee D. E., and Keller L. P. (1994) Reflectance spectroscopy of individual interplanetary dust particles. *Lunar Planet. Sci.* **25**, 159–160 (abstr.).

Brownlee D. E., Joswiak D. J., and Love S. G. (1993) Identification of cometary and asteroidal particles in stratospheric IDP collections. *Lunar Planet. Sci.* **24**, 205–206 (abstr.).

Brownlee D. E., Joswiak D. J., Schlutter D. J., Bradley J. P., and Love S. G. (1995) Identification of individual cometary IDPs by thermally stepped He release. *Lunar Planet. Sci.* **26**, (in press). (abstr.)

Clemett S. J., Maechling C. R., and Zare R. N. (1992) Analysis of polycyclic aromatic hydrocarbons in seventeen ordinary and carbonaceous chondrites. *Lunar Planet. Sci.* **23**, 233–234 (abstr.).

Appendix H:

S. Bajt., H.N. Chapman, G.J. Flynn and L.P. Keller, (1996) Carbon Characterization in Interplanetary Dust Particles With a Scanning Transmission X-Ray Microscope, (abstract) Lunar and Planetary Science XXVII, pages 57-58.

CARBON CHARACTERIZATION IN INTERPLANETARY DUST PARTICLES WITH A SCANNING TRANSMISSION X-RAY MICROSCOPE: S. Bajt[1], H. N. Chapman[2], G. J. Flynn[3] and L. P. Keller[4] (1) The University of Chicago, CARS, Chicago, IL 60637, (2) Dept. of Physics, SUNY-Stony Brook, Stony Brook, NY 11794, (3) Dept. of Physics, SUNY-Plattsburgh, NY 12901, (4) MVA Inc., 5500-200 Oakbrook Parkway, Norcross GA 30093.

Carbon XANES (X-ray Absorption Near Edge Spectroscopy) spectra of two carbon-rich interplanetary dust particles (IDPs) and a selected set of carbon standards were measured with a Scanning Transmission X-ray Microscope (STXM) to identify the carbon bonding in IDPs. The XANES spectra of three regions of one IDP (L2008 F4) show a notable similarity to the C-XANES spectrum of C_{60} (known also as buckminsterfullerene, or buckyballs). Efforts are underway to confirm the presence of C_{60} in this IDP using other analytical techniques and to exclude the possibility of contamination. The peak positions in the C-XANES spectrum of the second IDP, L2008 H9, suggest that carbon is present mainly as graphite or poorly-graphitized carbon.

IDPs are probably an important source of organic matter early in planetary evolution. These particles are small enough to be gently decelerated by the atmosphere and therefore the organic matter they deliver is relatively intact [1]. Thus, studies of the nature and distribution of carbon in IDPs can reveal important information about the prebiotic organic material on the early Earth. The first high-resolution x-ray images of carbon in one IDP and carbon XANES spectra have been presented elsewhere [2]. In this work we investigated two carbon-rich IDPs and measured several standards containing carbon in different forms. The experiments included x-ray imaging to obtain detailed carbon density maps and x-ray spectroscopy measurements to obtain chemical bonding information on a chosen spots in the sample.

The carbon imaging was done with 50 nm spatial resolution, using the STXM at the National Synchrotron Light Source. The sample is scanned through a monochromatic focused x-ray beam and the transmitted flux is detected by a proportional counter, which has a very low noise and high count rate capability. X-ray energies in the energy range from 250-330 eV were used for x-ray spectroscopic measurements. The flux at these energies is usually about 10^6 ph/s for a 0.5 eV energy resolution. A XANES spectrum of CO_2 gas with three sharp resonances, was utilized for energy calibration and was checked at the beginning and at the end of each experimental session. We measured two chondritic porous IDPs, L2008 F4 and L2008 H9. Both particles were embedded in sulphur, sectioned by ultramicrotomy and finally mounted on SiO membranes. The thin section of IDP L2008 F4 was 50-80 nm thick and L2008 H9 about 150 nm thick. We also measured spectra of pure materials that are known or have been proposed to exist in IDPs. These included graphite, partially graphitized carbon, $CaCO_3$, two polycyclic aromatic hydrocarbon (PAH) samples (pyrene - molecular weight 202 and dibenzoperylene -molecular weight 326, courtesy of S. J. Clemett from Stanford Univ.), and K-Fe-CN (Prussian blue pigment) where all carbon is triple-bonded to nitrogen. These standards were used to identify characteristic π^* and σ^* peaks in C-XANES spectra.

Previous work done on characterization of carbon-rich material in IDPs using TEM and SEM suggests that carbon is generally present either as poorly graphitized or amorphous carbon that occurs in anhydrous IDPs as grain coatings, as a matrix in certain fine-grained aggregates and as distinct clumps [3]. In hydrated IDPs carbonates were observed in minor amounts but the predominant phase was suggested to be amorphous or poorly-graphitized carbon [4]. The distribution of these carbon phases in hydrated IDPs is not known because it is difficult to differentiate poorly-ordered fine-grained carbonaceous materials from fine-

grained phyllosilicate which is abundant in hydrated IDPs. Clemett et al. [5] have reported finding many PAHs in IDPs measured with a laser microprobe but their locations (carriers) and abundances within the IDPs could not be determined.

Carbon images obtained with the STXM show that carbon is not uniformly distributed within the analyzed IDPs. Carbon XANES spectra were taken at different carbon-rich spots. XANES spectra of L2008 F4 are different from carbon XANES spectra of L2008 H9. Within the same IDP particle, carbon XANES spectra are typically very similar, however. XANES data of L2008 H9 show two peaks, at 285.6 and 288.9 eV, which correspond very well with the positions of graphite or partly graphitized carbon XANES peaks (Fig. 1). L2008 F4 particle exhibits three peaks at energies 284.8, 286.3 and 288.5 eV (Fig. 2). Three patches within this particle show the same peak positions within the experimental error (± 0.25 eV) with slight variation in their relative intensities. These peak energy positions are remarkably close to the peak energy positions of C_{60} XANES spectrum which are 284.3, 285.6, 286.0 and 288.2 eV. These energy positions are known from a published XANES spectrum acquired with an energy resolution of ± 0.1 eV [6]. In the spectrum of C_{60} there should be two peaks at 285.6 and 286.0 eV while we see only one peak centered at 286.3 eV. This could be because we could not resolve the two peaks. Even though fullerenes were not found in IDPs up to now there were reports on small concentrations of fullerenes found in carbonaceous meteorites [7], and therefore this finding would not be a complete surprise. Electron energy-loss spectroscopy obtained from additional thin sections of L2008 F4 also show multiple π^* peaks at the C K-edge. Of the ~ 20 IDPs analyzed to date using EELS, L2008 F4 is the only anhydrous IDP which shows a split π^* peak. Although this particle experienced exactly the same capture and sample preparation as other IDPs we can not completely exclude contamination at this point. Peak positions in C-XANES spectra of L2008 F4 are inconsistent with the peak positions characteristics for graphite, poorly graphitized carbon, carbide and the two PAHs. At this time we can also not exclude the possibility that some C-N-O compounds can produce peaks at these energies [8] however, N was not detected in thin sections of L2008 F4 using EELS.

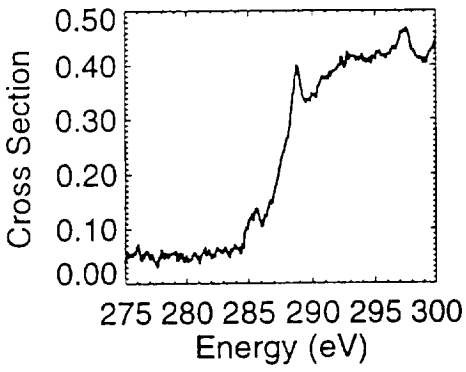

Figure 1: C-XANES of L2008 H9

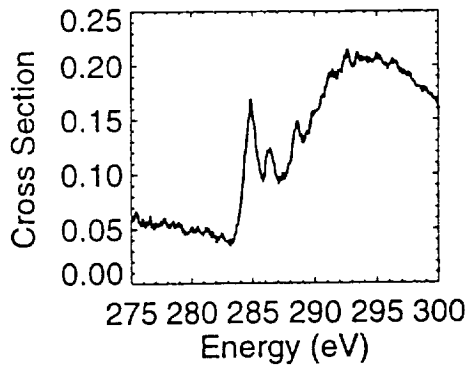

Figure 2: C-XANES of L2008 F4

References:

[1] Anders E., *Nature* **342** (1989) 255-257. [2] Chapman H. N. et al., *Meteoritics* **30** (1995) 496-497. [3] Thomas K. L. et al. (1994), in Analysis of Interplanetary Dust, AIP Conf. Proc. 310 (eds. M. E. Zolensky et al.), AIP Press, New York, pp. 165-171. [4] Keller L. P. et al., (1994), in Analysis of Interplanetary Dust, AIP Conf. Proc. 310 (eds. M. E. Zolensky et al.), AIP Press, New York, pp. 159-164. [5] Clemett S. J.et al., *Science* **262** (1993) 721-725. [6] Terminello L. J. et al., *Chem. Phys. Lett.* **182** (1991), 491-495. [7] Becker L. et al., *Nature* **372** (1994), 507. [8] Ade H. et al., *Science* **258**, 972-975.

G.J. Flynn, S. Bajt and S.R. Sutton, (1996) Evidence For Weakly Bound Bromine in Large Interplanetary Dust Particles Collected From The Stratosphere, (abstract) Lunar and Planetary Science XXVII, pages 367-368.

EVIDENCE FOR WEAKLY BOUND BROMINE IN LARGE INTERPLANETARY DUST PARTICLES COLLECTED FROM THE STRATOSPHERE:

G. J. Flynn[1], S. Bajt[2], and S. R. Sutton[2] (1) Dept. of Physics, SUNY-Plattsburgh, Plattsburgh NY 12901, (2) The University of Chicago, Chicago IL 60637

Bromine concentrations exceeding 100 times the CI meteorite value have been measured in interplanetary dust particles collected from the Earth's stratosphere. Because of the high halogen content and the long duration of particle residence in the stratosphere, Br contamination is possible. Six large interplanetary dust particles were analyzed using the Synchrotron X-ray Fluorescence Microprobe at the National Synchrotron Light Source. Each particle was exposed to the x-ray beam for a continuous 4 to 16 hour period. An approximately exponential decay of the Br content with time, over a 2-hour period, was observed. Since the particles are estimated to be heated to <100° C during these analyses, this easily mobilized Br is likely to be a contaminant. In all cases the Br concentration stabilized at a value which exceeded the CI meteorite value. No loss of S, CI, K, Cu, Zn, or Ge was observed, indicating tnat these elements are more strongly bound.

Since van der Stap et al. [1] reported large excesses of Br in interplanetary dust particles (IDPs) over the Br in CI meteorites, there has been concern that some or all of this excess Br might result from contamination. Mackinnon and Mogk observed thin (~150 Angstrom), S-rich surface layers on particles recovered from the Earth's stratosphere [2], suggesting contamination by stratospheric sulfuric acid aerosols. Since halogens are abundant in the atmosphere, Cl and Br contamination are possible.

Using the Synchrotron X-ray Fluorescence Microprobe at the National Synchrotron Light Source, we previously performed repeated chemical analyses of 3 large (>35 microns) IDPs [3]. The Br concentration decreased by ~50% from the first to the second analysis in 2 IDPs but no other element decreased, suggesting some of the Br in these IDPs was more weakly bound than any other element measured [3].

Experimental Procedure

Six large IDPs, each >35 microns, having chondritic compositions and classified as C-type in the JSC Catalog, were selected. To study the Br loss from IDPs in detail, each IDP was analyzed continuously for a period exceeding four hours. X-ray fluorescence spectra were collected sequentially over ~15 minute intervals. For these large IDPs, a 15 minute analysis is sufficient to determine the contents of elements present in concentrations greater than ~10 ppm, about a factor of four poorer sensitivity than obtained in the typical 2-hour IDP analysis using this X-ray Microprobe.

The first three IDPs (L2009H7, L2009F12, and L2008F17) were analyzed with a 170 micron thick aluminum filter between the sample and the energy dispersive x-ray detector. This filter absorbs lower energy x-rays minimizing the pile-up peaks from Fe and Ni, but it also precludes detection of light elements including S and Cl. We measured the Fe, Ni, Cu, Zn, and Br contents of these samples as a function of time.

To include light elements, particularly S and Cl, the 170 micron filter not used for analyses of the next three large IDPs (L2006E8, L2008E20 and L2009D5). Under these conditions, pile-up peaks interfere with the peaks of some elements heavier than Br. In these samples we measured S, Cl, K, Fe, Ni, Cu, Zn, Ge, and Br contents versus time.

Br Loss vs. Duration of Exposure to X-ray Beam

All of these IDPs except L2008E20 experienced significant Br loss. This loss followed the same basic pattern in all 5 cases: a constant Br content for the first ~60 minutes, a progressive loss of Br over the next ~120 minutes, and finally a stable Br concentration. In two cases overnight analyses (>12 hours duration) were performed, and no additional Br loss was observed. The most extreme Br loss was in L2009H7, which lost over 90% of its initial Br (see Figure 1). L2009F12 lost ~70% of its initial Br (see Figure 2), L2009D5 lost ~50% of its initial Br (see Figure 3), while L2008F17 and L2006E8 lost only ~30% of their initial Br. In all cases, the Br remaining after removal of the weakly-bound Br significantly exceeded the concentration in CI carbonaceous chondrites.

Figures 1, 2 and 3 show approximately exponential Br loss with time. The 60 minute delay before Br loss begins is puzzling, but might result from silicone oil surrounding the

Flynn, George
SUNY Plattsburgh - 54

IDPs. The results suggest there are at least two Br phases in these IDPs: a weakly bound phase mobilized by exposure to the x-ray beam, and a more tightly bound phase unaffected by the x-ray beam. X-ray beam heating is estimated to raise the temperature of these IDPs to no more than 100° C. If this loss of Br resulted from sample heating, then the low release temperature of the weakly bound Br is consistent with either an extermely volatile Br phase (Br_2 boils at 59° C) or surface adsorbed Br. In either case, it seems unlikely this weakly bound Br could have survived the heating pulse experienced by most IDPs on atmospheric entry [4], and thus it is likely to be a contaminant acquired after entry. We have not observed Br loss on the few smaller IDPs analyzed multiple times with this X-ray Microprobe, but further studies on small IDPs are in progress.

Other Volatile Elements

The volatile elements Cu, Zn, Ga, Ge and Se are also enriched, by factors of 1.5 to 3 over CI meteorite concentrations, in the IDPs collected from the stratosphere [5]. Jessberger et al. [6] suggest atmospheric contamination may cause these volatile enrichments. If significant quantities of these elements were deposited onto IDPs along with the weakly bound Br, then loss of these elements along with Br might occur.

The initial and final contents of Cu and Zn are identical, within the ±20% analysis errors, in all six IDPs, and there is no evidence for loss of Cu or Zn with time (see Figures 1, 2 and 3). The second set of IDPs provides a test for S, Cl, and K loss, and two of these particles also had Ge above detection limits. L2009D5 lost 50% of its initial Br, however, no loss of Cu, Zn, Ge, K, S, or Cl was detected (see Figure 3). Similar results were obtained for L2006E8, however, the Br loss in this particle was only 30%. Particle L2008E20 lost no Br, and the concentrations of the other volatile elements remained constant as well. These results demonstrate that essentially all of the Cu, Zn, Ge, S, Cl, and K is more strongly bound in these large IDPs than the weakly-bound Br component.

References: 1) van der Stap, C.C.A.H. et al., Lunar & Planet. Sci. XVII, 1013-1014. 2) Mackinnon, I.D.R. and Mogk, D.W. (1985) Geophys. Res. Lett., 12, 93-96. 3) Flynn, G.J. et al. (1995) Meteoritics, 30, 505. 4) Flynn, G.J. (1989) Proceedings 19th Lunar & Planet. Sci. Conf., 673-682. 5) Flynn, G.J. et al. (1993) Lunar & Planet. Sci. XXIV, 495-496. 6) Jessberger, E.K. et al. (1992) Earth Planet. Sci. Lett., 112-119.

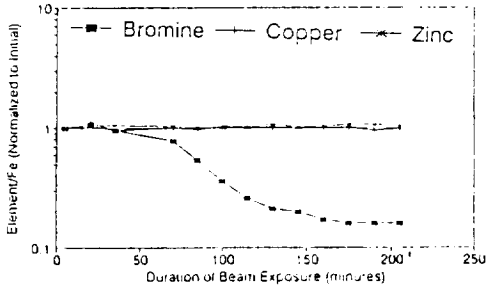

Figure 1: Br/Fe, Zn/Fe, and Cu/Fe in L2009H7.

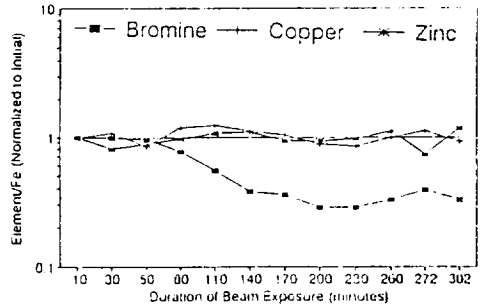

Figure 2: Br/Fe, Zn/Fe, and Cu/Fe in L2009F12.

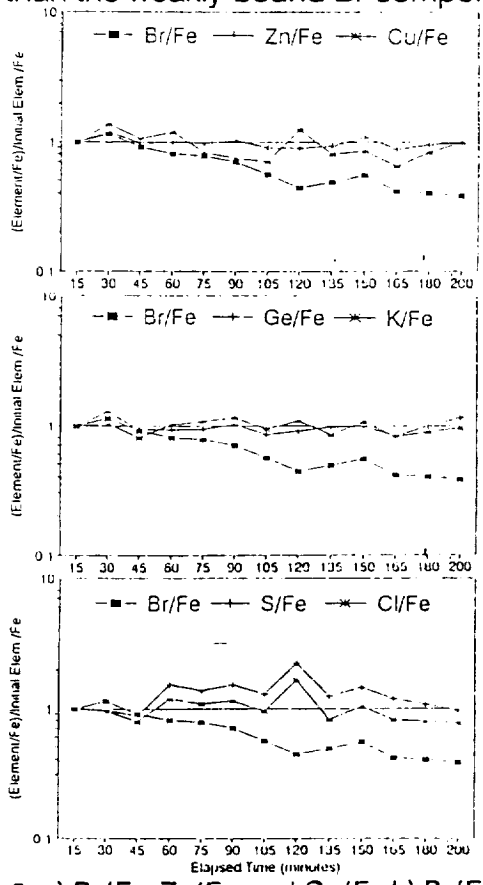

Figure 3: a) Br/Fe, Zn/Fe, and Cu/Fe b) Br/Fe, Ge/Fe, and K/Fe, and c) Br/Fe, S/Fe, and Cl/Fe vs. duration of exposure to the x-ray beam in L2009D5.

G.J. Flynn, (1996) Are the S-Type Asteroids the Parent Bodies of Ordinary Chondrite Meteeorites?: Evidence From The Interplanetary Dust Recovered From The Earths Stratosphere, (abstract) Lunar and Planetary Science XXVII, pages 365-366.

ARE THE S-TYPE ASTEROIDS THE PARENT BODIES OF ORDINARY CHONDRITE METEORITES?: EVIDENCE FROM THE INTERPLANETARY DUST RECOVERED FROM THE EARTH'S STRATOSPHERE:

G. J. Flynn, Dept. of Pnysics, SUNY- Plattsburgh, Plattsburgh NY 12901

The observation of dust bands associated with the Koronis family of S-type asteroids demonstrates that this family produces abundant interplanetary dust. Because of the low inclinations and eccentricities of the orbits of Koronis family members, dust from the Koronis family is enhanced in near-Earth collections. Kortenkamp et al. [1] estimate that the Koronis family and the C-type Themis family together contribute 55% of the interplanetary dust particles (IDPs) incident on the Earth. Comparison of the chemical, physical, and mineralogical properties of the IDPs collected in the stratosphere with those properties of ordinary chondrite meteorites show few similarities, suggesting the S-type Koronis asteroids produce IDPs distinctly different in composition and structure from ordinary chondrites and that these S-asteroids are not parent bodies of ordinary chondrite meteorites.

Comparison of astroncmical reflection spectra of asteroids with laboratory reflection spectra of meteorites has produced plausible identifications of parent bodies for most types of meteorites. However, the ordinary chondrites, the most abundant type of meteorite among the terrestrial falls, have no spectral match among the asteroids. It has been suggested that surface weathering might alter the reflection spectra of S asteroids, and that S-type asteroids may be parent bodies of the ordinary chondrite meteorites.

The Koronis family of S-type asteroids is associated with a major dust band, identified by the IRAS spacecraft, and is thus a known contributor to the interplanetary dust. Because of the low inclinations and eccentricities of the orbits of Koronis family members, gravitational focusing results in a significant enhancement of the flux of dust from the Koronis family near the Earth. Kortenkamp et al. [1] modeled the dust contributions from the bands detected by IRAS, and concluded that 55% of the interplanetary dust particles (IDPs) incident on the Earth are derived from the S-type Koronis family and the C-type Themis family of asteroids. Thus, we should expect a significant fraction, perhaps one-quarter, of the IDPs collected from the Earth's stratosphere to be derived from the S-type Koronis family. If so, detailed comparison of the chemical compositions, mineralogies, and physical properties (eg. grain size, porosity, and density) of the IDPs from the Earth's stratosphere with those properties of the ordinary chondrite meteorites should resolve the question: "Are the S-type asteroids the parent bodies of the ordinary chondrites?"

Comparison of IDPs with Ordinary Chondrite Meteorites

The IDPs collected from the Earth's stratosphere range from ~5 to >50 microns in diameter. Preliminary characterization (EDX spectra, optical properties and sizes) of these stratospheric particles is performed at the NASA Johnson Space Center, and individual particles are then made available for detailed analysis. A large majority of these IDPs have major element compositions (Mg, Al, Si, Ca, Cr, Fe, and Ni) similar to chondritic meteorites. These chondritic IDPs are similar to ordinary chondrites in major refractory elements. However, the carbon contents measured in all 71 chondritic IDPs analyzed by Thomas et al. [2] and an additional 30 chondritic IDPs by Schramm et al. [3] each significantly exceed the carbon content of any type of ordinary chondrite meteorite. The volatile elements S, Na, P, K, Cu, Zn, Ga, Ge, Se, and Br are also more abundant in most chondritic IDPs than in ordinary chondrites [4].

Bradley et al. [5] measured the visible and near-infrared reflection spectra, from 380 to 800 nm, of five individual chondritic IDPs. Some of these IDPs had flat reflection spectra, similar to the C-type asteroids, while others showed a pronounced rise in reflectivity in the red, similar to the P-type or D-type asteroids, and most chondritic IDPs appear black when viewed in the optical microscope. Both the spectral shapes and the low albedos of these IDPs are inconsistent with the observed spectra and albedos of S-type asteroids.

The chondritric IDPs are generally extremely fine-grained (typical grain size <1 micron), have significant porosity, and many contain unequilibrated mafic silicates. The ordinary chondrites, on the other hand, are coarse-grained, have low porosity, and are generally well equilibrated. Thus, most (or all) of the chondritic IDPs are chemically, mineralogically, physically, and spectrally different from the ordinary chondrite meteorites.

Flynn, George
SUNY Plattsburgh - 56

IDPs. The results suggest there are at least two Br phases in these IDPs: a weakly bound phase mobilized by exposure to the x-ray beam, and a more tightly bound phase unaffected by the x-ray beam. X-ray beam heating is estimated to raise the temperature of these IDPs to no more than 100° C. If this loss of Br resulted from sample heating, then the low release temperature of the weakly bound Br is consistent with either an extermely volatile Br phase (Br_2 boils at 59° C) or surface adsorbed Br. In either case, it seems unlikely this weakly bound Br could have survived the heating pulse experienced by most IDPs on atmospheric entry [4], and thus it is likely to be a contaminant acquired after entry. We have not observed Br loss on the few smaller IDPs analyzed multiple times with this X-ray Microprobe, but further studies on small IDPs are in progress.

Other Volatile Elements

The volatile elements Cu, Zn, Ga, Ge and Se are also enriched, by factors of 1.5 to 3 over CI meteorite concentrations, in the IDPs collected from the stratosphere [5]. Jessberger et al. [6] suggest atmospheric contamination may cause these volatile enrichments. If significant quantities of these elements were deposited onto IDPs along with the weakly bound Br, then loss of these elements along with Br might occur.

The initial and final contents of Cu and Zn are identical, within the ±20% analysis errors, in all six IDPs, and there is no evidence for loss of Cu or Zn with time (see Figures 1, 2 and 3). The second set of IDPs provides a test for S, Cl, and K loss, and two of these particles also had Ge above detection limits. L2009D5 lost 50% of its initial Br, however, no loss of Cu, Zn, Ge, K, S, or Cl was detected (see Figure 3). Similar results were obtained for L2006E8, however, the Br loss in this particle was only 30%. Particle L2008E20 lost no Br, and the concentrations of the other volatile elements remained constant as well. These results demonstrate that essentially all of the Cu, Zn, Ge, S, Cl, and K is more strongly bound in these large IDPs than the weakly-bound Br component.

References: 1) van der Stap, C.C.A.H. et al., Lunar & Planet. Sci. XVII, 1013-1014. 2) Mackinnon, I.D.R. and Mogk, D.W. (1985) Geophys. Res. Lett., 12, 93-96. 3) Flynn, G.J. et al. (1995) Meteoritics, 30, 505. 4) Flynn, G.J. (1989) Proceedings 19th Lunar & Planet. Sci. Conf., 673-682. 5) Flynn, G.J. et al. (1993) Lunar & Planet. Sci. XXIV, 495-496. 6) Jessberger, E.K. et al. (1992) Earth Planet. Sci. Lett., 112-119.

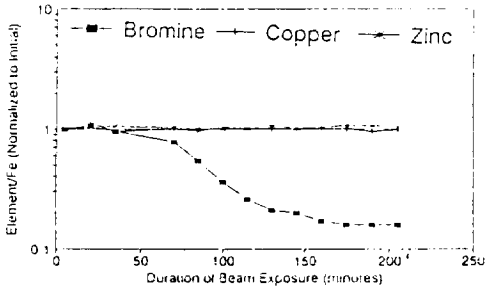

Figure 1: Br/Fe, Zn/Fe, and Cu/Fe in L2009H7.

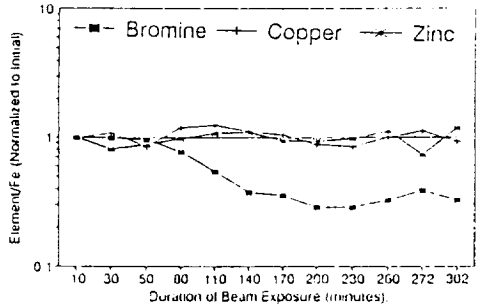

Figure 2: Br/Fe, Zn/Fe, and Cu/Fe in L2009F12.

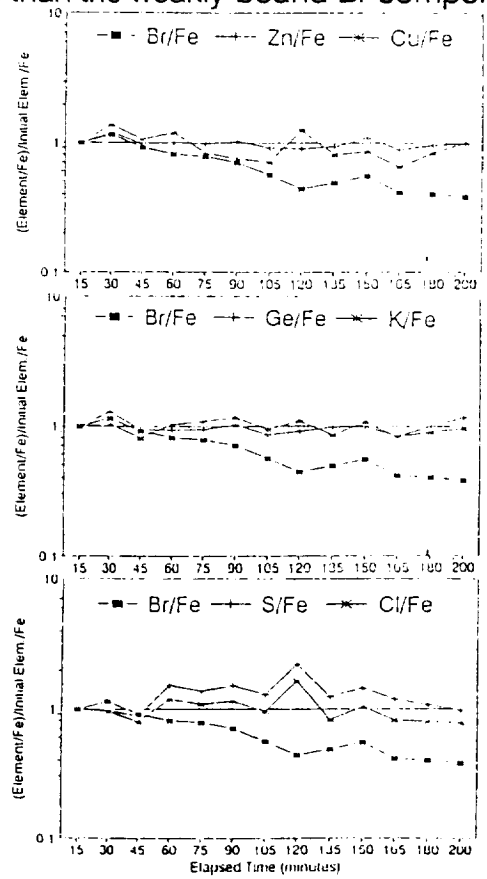

Figure 3: a) Br/Fe, Zn/Fe, and Cu/Fe b) Br/Fe, Ge/Fe, and K/Fe, and c) Br/Fe, S/Fe, and Cl/Fe vs. duration of exposure to the x-ray beam in L2009D5.

G.J. Flynn, F. Horz, S. Bajt, and S.R. Sutton, (1996) In-Situ Chemical Analysis of Extraterrestrial Material Captured in Aerogel, (abstract) Lunar and Planetary Science XXVII, pages 369-370.

IN-SITU CHEMICAL ANALYSIS OF EXTRATERRESTRIAL MATERIAL CAPTURED IN AEROGEL:

G. J. Flynn[1], F. Horz[2], S. Bajt[3], and S. R. Sutton[3] (1) Dept. of Physics, SUNY-Plattsburgh, Plattsburgh NY 12901, (2) NASA Johnson Space Center, Houston TX 77058, (3) The University of Chicago, Chicago IL 60637

High-speed interplanetary dust and orbital debris can be collected non-destructively using aerogel capture cells on earth-orbiting spacecraft and the STARDUST comet sample return mission. In-situ chemical analysis of captured particles is highly desirable for initial classification as space debris or interplanetary dust, allowing quick determination of the dust to debris ratio, and selection of an appropriate analytical protocol for each particle based on a prior knowledge of its type. In a proof-of-principle experiment the X-Ray Microprobe at the National Synchrotron Light Source was used to analyze 50 micron diameter Allende fragments shot into 20 mg/cc silica aerogel at 3 to 6 km/s. A one-second data acquisition allowed determination of Fe/Ni ratios. Five minute data acquisitions allowed analysis of Fe, Ni, Cu, and Zn in Allende fragments as deep as 5 mm below the aerogel surface and Ca was detected in fragments up to 3.6 mm below the surface, demonstrating the ability to identify chondritic material, and distinguish it from orbital debris, by in-situ chemical analysis.

The intact capture of hypervelocity dust particles into aerogel has been demonstrated and aerogel collectors have been flown on earth-orbital space missions [1, 2]. The particles collected in earth orbit include both man-made space debris and interplanetary dust. In-situ chemical analysis of the captured particles would provide a preliminary characterization allowing: 1) rapid determination of the ratio of interplanetary dust to space debris in each size range, and 2) assignment of a specific analytical protocol to each particle based on a prior knowledge of its status as debris or interplanetary dust.

To simulate orbital capture, 43 to 56 micron fragments of the Allende carbonaceous chondrite were launched at 3 to 6 km/s into slabs of silica aerogel having a density of 20 mg/cc, using a 5mm light gas gun. Many of the initial projectiles fragmented during launch, causing a diversity of track lengths. The variable burial depth and fragment mass allowed determination of the feasibility and limitations of in-situ analysis.

The X-ray Microprobe at the National Synchrotron Light Source at Brookhaven National Laboratory, which uses a white-light x-ray beam of approximately 8 microns diameter for excitation, is suitable for in-situ chemical analysis of particles collected in aerogel [3]. Unlike electron microprobes, where the incident beam penetrates to only tens of microns, the highest energy x-rays in this incident beam penetrate several centimeters into low density aerogel. Thus, using the X-ray Microprobe, the detection of an element is dependent on the depth from which the fluorescence x-rays can escape the aerogel rather than on the depth to which the incident beam can penetrate. The X-ray Microprobe analysis is essentially non-destructive, and any sample alteration should be far less severe than that experienced during capture in the aerogel.

Chemical analysis was performed with the incident x-ray beam at a 45° angle to the surface of the aerogel and with an energy dispersive x-ray detector at a 90° angle to the incident beam (see Figure 1). A video microscope with a 5x, long-working-distance objective was located perpendicular to the surface of the aerogel. The sample was mounted on a 3-axis moveable stage, allowing vertical and horizontal motions to center individual particles in the x-ray beam, and motion parallel to the axis of the video camera.

The video system provided sufficient resolution to follow each track from the surface of the aerogel to its termination point. We examined six tracks which had Allende particles at their ends. The depth of each particle beneath the surface of the aerogel was measured by focusing the video microscope on the surface of the aerogel, then moving

Table 1: In-Situ Analyses - Allende Particles Captured in Aerogel

Particle	Depth Below Surface	Elements Detected
Allende 1	3.4 mm	Ca, Cr, Fe, Ni, Cu, Zn
Allende 2	3.0 mm	Ca, Cr, Fe, Ni, Cu, Zn
Allende 3	3.6 mm	Ca, Cr, Fe, Ni, Cu, Zn
Allende 4	4.5 mm	Fe, Ni, Cu, Zn
Allende 5	4.9 mm	Fe, Ni, Cu, Zn
Allende 6	1.1 mm	Ca, Ti, Cr, Fe, Ni, Cu, Zn

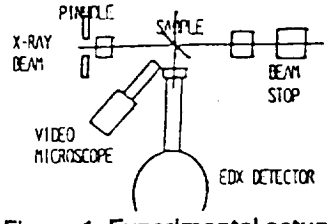

Figure 1: Experimental setup.

the sample in 0.01 mm increments until the Allende fragment came into focus. (The index of refraction of aerogel is sufficiently close to air that no correction was made.) The six fragments ranged in depth from 1.1 to 4.9 mm below the surface (see Table 1).

Chemical analysis of the aerogel showed a major peak at Si, consistent with the composition of aerogel, and a large Ar peak due to Ar in the air along the incident beam path (see Figure 2a). Calcium and Fe were also detected in this aerogel. The Ca in this aerogel may be sufficient to preclude quantitative determination of the Ca contents of some of the Allende samples, emphasizing the importance of selecting aerogels which have a minimum of contamination for particle capture experiments [3, 4].

When an Allende fragment was centered in the incident x-ray beam, strong signals were detected at the Fe and Ni K-alpha and K-beta fluorescence energies. Zinc, and Cu were also detected in all six Allende particles. The volatile elements Cu and Zn provide an unambigous discrimination between most man-made NiFe (with low Zn contents) and chondritic material (with several hundred ppm of both Zn and Cu). Even the deepest particle, Allende 5 (analyzed at a depth of 4.9 mm below the surface), showed clear signals of the Zn and Cu (see Figure 2b). The high Zn and Cu contents suggest little loss of these moderately volatile elements during capture. The observed count rates indicate the current X-ray Microprobe could perform in-situ chemical analysis of particles as small as 5 microns in 15 to 30 minutes.

Fluorescence signals are attenuated during passage through the aerogel, thus the X-ray Microprobe can detect high-Z elements, such as Fe and Ni, at significantly greater depths than elements of lower Z, eg. Ca. Figure 2c shows Ca detection in Allende 6, 1.1 mm below the surface of the aerogel. Very small Ca signals were seen in Allende 1, Allende 2, and Allende 3, at depths of 3.0 to 3.6 mm, but no Ca was detected in Allende 4 or Allende 5, at depths of 4.5 and 4.9 mm below the surface of the aerogel. If the Ca contents of the 6 Allende particles are all similar, this result suggests our maximum sampling depth for Ca in aerogel of density 20 mg/cc is of order 4 mm.

Since typical meteoroids travel about 100 projectile diameters before stopping in 20 mg/cc aerogel [2], particles up to ~10 microns in diameter should stop within 1 mm of the aerogel surface, while 50 micron particles should stop within 5 mm of the surface.

To determine the minimum time required to identify a chondritic particle, one-second data acquisitions were performed on Allende 2 and on the aerogel about 300 microns from Allende 2. Both Ni and Fe were detected in Allende 2 in one-second, indicating we can identify a chondritic particle and determine its Ni/Fe ratio with a data acquisition time of less than one second. Thus a mapping experiment to locate all chondritic particles in an aerogel sample would require no longer than one second per pixel in the map.

These results demonstrate that the X-ray Microprobe can perform in-situ chemical analyses of interplanetary dust and orbital debris captured in aerogel. Chondritic material can be identified, and metallic debris containing iron, copper or other high-Z elements can be distinguished from chondritic material, at depths exceeding 5 mm in 20 mg/cc aerogel. The X-ray Microprobe can also provide in-situ chemical characterization of particles captured in aerogel on comet sample return missions, such as STARDUST.

References: 1) Tsou, P. et al. (1993) Lunar & Planet. Sci. XXIV, 1443-1444. 2) Brownlee, D. E. et al. (1994) Lunar & Planet. Sci. XXV, 183-184. 3) Flynn G.J. and Sutton, S.R. (1994) in Workshop on Particle Capture, Recovery, and Velocity/Trajectory Measurement Technologies, LPI, Houston, 36-37. 4) Barrett et al. (1992) Proc. 22nd Lunar Planet. Sci. Conf., LPI, Houston, 203-212.

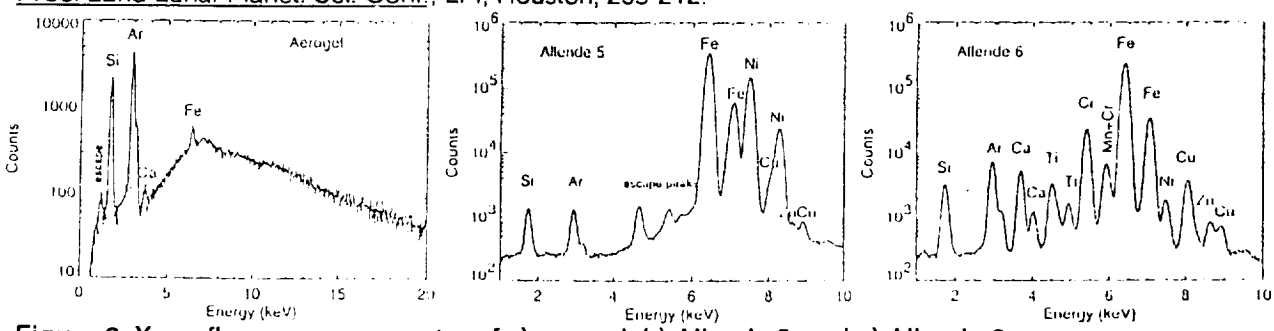

Figure 2: X-ray fluorescence spectra of a) aerogel, b) Allende 5, and c) Allende 6.

Appendix L: Flynn, G. J. (1996) The Contribution of Volatiles to the Surface and Atmosphere of Mars by the Accretion of Interplanetary Dust Particles, (abstract) Workshop on the Evolution of Martian Volatiles, LPI Tech Report 96-01, LPI Houston, 14-15.

THE CONTRIBUTION OF VOLATILES TO THE SURFACE AND ATMOSPHERE OF MARS BY THE ACCRETION OF INTERPLANETARY DUST PARTICLES. G. J. Flynn, Department of Physics, State University of New York–Plattsburgh, Plattsburgh NY 12901, USA.

The accretion of interplanetary dust particles (IDPs), comets, and meteorites provides a continuous addition of volatiles, including water, organics, and noble gases, to the surface and atmosphere of Mars after its formation and differentiation. The magnitude of these contributions can be estimated from the observed contributions to the Earth and Moon.

The mass distribution of extraterrestrial matter accreted by the Earth shows a bimodal distribution, sharply peaked at 10^{-7} g and 10^{18} g. The lower mass peak corresponds to the continuous, planetwide accretion of IDPs (derived from comets and asteroids), while the higher mass peak results from the infrequent impact of kilometer-size objects. Since the areas under both peaks are similar, the IDPs and the large impactors each contribute comparable masses of material to the Earth. If the IDPs and large impactors have the same composition, then each will carry roughly the same amount of water and organics to the surface. However, accretion of volatiles by the large impactors is hampered by vaporization, and possible escape, due to impact heating. IDPs, on the other hand, are gently decelerated in the atmosphere of Earth or Mars, and many IDPs arrive at the surface with their volatiles intact.

The IDPs carry with them solar wind ions, implanted while they are in space, producing concentrations of noble gases that exceed the noble gas concentrations in meteorites by several orders of magnitude. Thus, IDPs are likely to make a significantly larger contribution to the noble gas inventory of Mars than is made by the impact of the same mass of large asteroidal fragments.

Interplanetary Dust Accretion Onto Mars: The present rate of accretion of IDPs onto Mars was estimated from the flux measured at Earth using techniques described by Flynn and McKay [1]. Using this method, about 12×10^9 g of IDPs accrete onto Mars annually [2], about 75% of the 16×10^9 g/yr accreting onto the Earth [3].

Water. The chemical composition of the meteoritic component in lunar soils most closely resembles that of the CI carbonaceous chondrites [4], which have water contents ranging from 18% to 22% [5]. No quantitative water measurements have been performed on the IDPs collected at Earth, but mineralogical examination indicates that about half these IDPs contain significant abundances of hydrated silicates, the dominant water-bearing phase in CI meteorites. Taking the water abundance in the IDPs as 20%, the mean for CI meteorites, IDPs contribute about 2.4×10^9 g/yr of water, resulting in a average surface coverage of 2×10^{-9} g/cm^2 yr. Over the last 3.6 b.y. this would produce a layer of water about 7 cm thick over the entire surface of Mars.

Carbon. The C contents of CI meteorites range from 3% to 5% [5], but IDPs collected from the Earth's stratosphere have a mean C content of about 12% [6]. Using the 12% value, IDPs contribute about 1.5×10^6 kg/yr of C to the surface of Mars, or about 6×10^{15} kg of C over the last 3.6 b.y.

Noble gases. The indigenous noble gas content of meteoritic material is quite low; however, IDPs acquire noble gases from solar wind irradiation while in space. Isotopic abundances of Ne, Ar, and Xe were measured on a group of 13 IDPs from the stratosphere [7] and He and Ne abundances have been measured on 82 individual IDPs [8]. The IDP contribution of noble gases to Mars (in Table 1) were calculated assuming these IDPs have the same noble gas concentrations as those collected from the stratosphere of Earth.

TABLE 1. Noble gas contribution by IDPs.

Isotope	Accretion Rate (cc STP/yr)	Mass Accreted Over 3.6 b.y. (g)
^{3}He	1.4×10^6	7×10^{11}
^{4}He	3.6×10^8	3×10^{14}
^{20}Ne	5.3×10^6	2×10^{13}
^{22}Ne	4.8×10^5	2×10^{12}
^{36}Ar	5.9×10^5	4×10^{12}
^{38}Ar	1.2×10^5	8×10^{11}
^{132}Xe	1.2×10^3	3×10^{10}

Accretion in the First Billion Years: The flux of large objects, capable of producing kilometer-sized craters, was significantly higher during the first billion years of solar system history than at present. Little is known about the flux of IDPs in that early era; however, collisions between the large asteroids and comets that produced the craters must have resulted in an abundance of dust. The accretion of meteoritic matter onto the Moon has been fit by a two-component model: a rapidly decaying flux ($t_{1/2}$ = 40 m.y.) exceeding the present flux by an order of magnitude or more 4 b.y. ago, and a relatively constant flux, near the present value, over the past 3.6 b.y. [9]. Using this model, the total accretion of IDPs from 4.0 b.y. to 3.6 b.y. ago would be about 30% of that from 3.6 b.y. to the present.

Extrapolating farther back in time, the contribution in the 200-m.y. interval from 4.2 to 4.0 b.y. ago would have been 5× that during the entire interval from 3.6 b.y. to the present. During the period from 4.5 b.y. to 4.0 b.y. ago, Mars could have acquired several meters of water, tens of centimeters of carbonaceous material, and a large inventory of noble gases from the accretion of IDPs.

References: [1] Flynn G. J. and McKay D. S. (1990) *JGR, 95*, 14497–14509. [2] Flynn G. J. (1995) in *Proceedings of the Small Bodies in the Solar System and Their Interactions with the Planets*, in press. [3] Hughes D. W. (1978) in *Cosmic Dust*, 123–185, Wiley. [4] Anders E. et al. (1973) *The Moon, 8*, 3–24. [5] Wasson J. T. (1985) *Meteorites*, 31, Freeman. [6] Thomas K. L. et al. (1994) in *Analysis of Interplanetary Dust*, 165–172, AIP Press. [7] Hudson B. et al. (1981) *Science, 211*, 383–386. [8] Nier A. O. (1994) in *Analysis of Interplanetary Dust*, 115–126, AIP Press. [9] Wasson J. T. et al. (1973) *The Moon, 13*, 121–141.

THE ABUNDANCE PATTERN OF ELEMENTS HAVING LOW NEBULAR CONDENSATION TEMPERATURES IN INTERPLANETARY DUST PARTICLES: EVIDENCE FOR A NEW CHEMICAL TYPE OF CHONDRITIC MATERIAL

G. J. Flynn
Dept. of Physics, SUNY-Plattsburgh, Plattsburgh NY, 12901

S. Bajt
Center for Advanced Radiation Sources, The University of Chicago, Chicago IL 60637

S. R. Sutton
Dept. of Geophysical Sciences, The University of Chicago, Chicago IL 60637

M. E. Zolensky
NASA Johnson Space Center, Houston TX 77058

K. L. Thomas
Lockheed-Martin, Houston TX, 77058

L. P. Keller
MTA Associates, Norcross GA, 30093

Abstract. The abundances of Ni, Fe, Cr, Mn, P, Cu, K, Na, Ga, Ge, Se, Zn, S, Br, and C were measured in interplanetary dust particles (IDPs) collected from the Earth's stratosphere. All elements with nebular condensation temperatures lower than Mn, except S, were enriched relative to the most volatile-rich type of meteorite while the refractory elements Cr and Ni were present at chondritic abundances. This element abundance pattern is consistent with nebular condensation, suggesting the IDPs condensed at either a different location or time in the evolving solar nebula than do the meteorites. The enrichments of the major elements C, Na, P, and K exclude the possibility that the volatile enrichment in IDPs results from a minor amount of contamination.

1. Introduction

Interplanetary dust particles (IDPs) from 5 to 50 microns in diameter are decelerated in the upper atmosphere and recovered from the Earth's stratosphere by NASA sampling aircraft (Warren & Zolensky, 1994). The majority of these IDPs are believed to be samples of asteroids and comets, though contributions from all solar system objects as well as interstellar dust are possible.

The abundances of refractory elements are generally similar among all types of chondritic meteorites, but abundances of elements with low nebular condensation temperatures decrease significantly increasing petrologic grade (see Figure 1). For example, carbon decreases systematically, by almost an order-of-magnitude, with increasing petrologic grade from CI(1) to CV(3) meteorites. Thus, the pattern of abundances of elements having low nebular condensation temperatures can distinguish between different types of chondritic material.

Those IDPs which are not dominated by single minerals (olivines, pyroxenes, or Fe-Ni-sulfides) have abundances of the major refractory elements which are similar, within ± 50%, to the chondritic meteorites. Schramm et al. (1989) demonstrated that the average content of major refractory elements (Mg, Al, Si, Fe, and Ni) in a set of 200 IDPs is approximately chondritic.

Volatile elements in these chondritic IDPs are generally enriched relative to the CI meteorites, which are believed to represent solar composition (Anders & Ebihara, 1982). Van der Stap et al. (1986) reported enrichments of 6 volatile trace elements in 3 IDPs examined by Proton Induced X-ray Emission, and suggested the IDPs sampled the volatile-rich residue of solar system formation. Flynn et al. (1993) found average enrichments by factors of 1.5 to 3 relative to CI for the volatile elements Cu, Zn, Ga, Ge, and Se and a larger enrichment for Br in a set of 51 IDPs. However, Arndt et al. (1995) noted these volatile enrichments are larger for the elements having the lowest abundances, and suggested that the apparent volatile enrichment could indicate a limit of detection problem, in which the abundances of elements near the detection limit are systematically overestimated, or could result from contamination, which requires only a small amount of non-indigenous material for the elements present in low abundances.

2. Measurement Techniques and Samples

The abundances of Cr, Mn, Fe, Ni, Cu, Zn, Ga, Ge, Se, and Br were measured in 51 IDPs using the Synchrotron X-ray Fluorescence Microprobe on Beamline X-26 of the National Synchrotron Light Source at Brookhaven National Laboratory. This X-ray Microprobe has a sensitivity of 1 to 3 ppm, in 10 micron chondritic particles, for elements from Fe to Sr. Abundances of Fe, Na, S, and C were measured on 71 IDPs using a scanning electron microscope equipped with a thin-window energy dispersive x-ray detector. The C detection limit is ~0.5%, while limits for Na, and S are ~0.1%. Abundances of Fe, K, Na, P and S were measured on 27 IDPs using an electron microprobe, with a detection limit of ~0.1%.

The IDPs analyzed range from 5 to 35 microns in size. These IDPs were collected from the stratosphere into silicone oil, which is impossible to remove completely, so the element abundances are normalized to Fe rather than Si. To minimize selection biases, all chondritic IDPs, i.e. all particles with contents of Mg, Al, Si, Fe, and Ni within a factor of two of CI, are included in the averages.

Some of these IDPs have been examined in the Transmission Electron Microscope (TEM) to determine mineralogy and texture. Each set includes both anhydrous and hydrated IDPs. Some of these IDPs show well-developed magnetite rims, indicating they experienced severe atmospheric entry heating while others have textures and mineralogies indicating less severe atmospheric entry heating (Flynn et al., 1992, Keller et al., 1995). Since the loss of Zn (Flynn et al. 1992) and S (Fraundorf et al. 1983) has been linked to severe atmospheric entry heating, the abundances of the volatile elements measured in this work may underestimate the preatmospheric volatile contents of some IDPs.

Appendix M:
Flynn, George
SUNY Plattsburgh - 60
Appendix M: Flynn, G.J. (1996) The Abundance Pattern of Elements Having Low Nebular Condensation Temperatures in Interplanetary Dust Particles: Evidence for a New Chemical Type of Chondritic Material, IAU Symposium, 150, in press.

3. Results

The abundances of most individual elements vary by an order-of-magnitude in each set of IDPs. This could be due either to the sampling of a multitude of chemically distinct parent objects (Schramm et al., 1989) or to heterogeneous distribution of these elements on the 10 micron scale in the parent body. Similar results are seen when individual fragments, up to 100 microns in size, of chondritic meteorites are measured by the same techniques, indicating significant heterogeneity of the meteorite parent bodies.

The CI and Fe normalized average element contents of the IDPs are shown in Figure 1. Sulfur and Na were measured on both the 27 and the 71 IDP sets. The S averages on the 27 and the 71 IDP sets are identical within errors, but the Na content is a factor of two higher in the 71 particle set. This could indicate the sample sets are too small to obtain a representative average over inhomogeneously distributed Na, or that Na is sufficiently volatile to be lost by to sample heating during the electron microbeam analysis.

All the elements with nebular condensation temperatures lower than Mn (~1170 K) show enrichments by factors from 1.5 to 5xCI, except for Br which is enriched over CI by a factor of 40 and S which is present at the CI concentration. Carbon, the major element having the lowest nebular condensation temperature of the set analyzed, is enriched by a factor of 3 over CI. Overall, the enrichment pattern seen in these IDPs is suggestive of a mirror image of the depletion pattern relative to CI for the CM(2) and CV(3) meteorites (see Figure 1).

4. Conclusions

The enrichments of both major (C, Na, K, P) and trace elements (Cu, Zn, Ga, Ge, Se, and Br) in IDPs demonstrate that the volatile enrichment previously reported for only the trace elements (Flynn et al. 1993) does not result from either a limit of detection problem or contamination of those elements present in the lowest abundances. The trace elements Cu and Zn are typically present at ~100 times the detection limit of the X-ray Microprobe, and only one particle in the 51 IDP set has a Zn abundance near the detection limit. Jessberger et al. (1992) suggest all of the enrichment above CI levels could result from contamination acquired during atmospheric residence of weeks to months. For contamination to explain these enrichments, those IDPs which contain the highest abundances of C, Na, and K would have to consist of more than 50% contaminant material, and the average IDP would have to consist of about 10% contaminant material. Such extreme levels of contamination should be discernible in the mineralogical and textural examination of IDPs in the TEM. Although Rietmeijer (1995) has found evidence of KCl surface contamination in one IDP, no obvious contamination of the magnitude required to explain these enrichments has been observed.

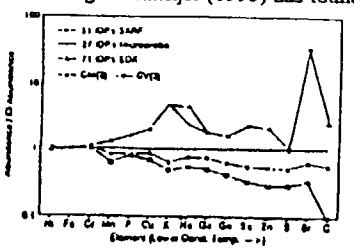

Figure 1: Average Fe and CI normalized abundances of elements in chondritic IDPs, CM(2), and CV(3) meteorites. Elements are ordered with decreasing nebular condensation temperature to the right.

Nonetheless, contamination of trace elements cannot be excluded. Mackinnon and Mogk (1985) have detected a thin (~150 angstrom) S-rich layer on the surface of some particles from the stratosphere, but the total mass of S in this layer is inadequate to significantly perturb the bulk S in IDPs. Flynn et al. (1995) have demonstrated that ~50% of the Br in 2 IDPs is very weakly bound and Stephan et al. (1994) found a halogen-rich rim on one IDP. These results suggest that a significant portion of the Br enrichment may result from contamination, most likely acquired during stratospheric residence.

Each of the chondritic IDPs included in this study has a carbon content greater than any carbonaceous chondrite. In comparison, stony meteorites are dominated by the carbon-poor ordinary chondrites. This indicates the chondritic IDPs sample a different, more carbon-rich, reservoir than that sampled by the stony meteorites.

The IDPs included in this study are, on average, more volatile-rich than the most volatile-rich meteorites, the CI chondrites, in a pattern indicative of nebular condensation. This suggests the IDPs, or some subset of the IDPs, are a new chemical type of extraterrestrial material, not sampled by the meteorites. This conclusion is consistent with TEM observations, which have demonstrated that most IDPs are mineralogically distinct from meteorites, and a large subset of the IDPs are mineralogically more primitive (i.e., exhibit less thermal and aqueous alteration) than any type of chondritic meteorite (Mackinnon and Rietmeijer, 1987). This is consistent with the suggestion of van der Stap. et al. (1986) that the IDPs formed during a late stage of nebular condensation, when some elements with high condensation temperatures had already been depleted in the gas phase.

References

Anders, E. & Ebihara, M. 1982, Geochim. Cosmochim. Acta, 46, 2363-2380.
Arndt, P. Maetz, M. & Jessberger, E. K. 1995, Meteoritics, 30 483.
Fraundorf, P., Brownlee, D. E. & Walker, R. M. 1983, in Comets (ed. L. L. Wilkening) Univ. of Arizona Press, Tucson, 383-412.
Flynn, G. J., Sutton, S. R., Thomas, K. L., Keller, L. P., & Klock, W. 1992, Lunar & Planet. Sci. XXIII, 375-376.
Flynn, G.J., Sutton, S.R. & Bajt, S. 1993, Lunar & Planet. Sci. XXIV, 497-498.
Flynn, G.J., Bajt, S., Sutton, S.R., and Klock, W. 1995, Meteoritics, 30, 505.
Jessberger, E.K., Bohsung, J., Chakaveh, S., & Traxel, K. 1992, Earth Planet. Sci. Lett., 112, 91-99.
Keller , L.P., Thomas, K.L. & McKay, D.S. 1995, "Mineralogical Changes in IDPs Resulting from Atmospheric Entry Heating," this volume.
Mackinnon, I.D.R. & Mogk, D.W. 1985, Geophys. Res. Lett., 12, 93-96.
Mackinnon, I.D.R. & Rietmeijer, F. 1987, Rev. of Geophys., 25, 1527-1553.
Rietmeijer, F.J.M. 1995, Meteoritics, 30, 33-41.
Schramm, L.S., Brownlee, D.E. & Wheelock, M. 1989, Meteoritics, 24, 99-112.
Stephan, T. , Jessberger, E.K., Rulle, H., Thomas, K.L., and Klock, W. 1994, Lunar & Planet. Sci. XXV, 1341-1342.
van der Stap, C. C. A. H., Vis, R. D., & Verheul, H. 1986, Lunar & Planet. Sci. XVII, 1013-1014.
Warren, J. L., and Zolensky, M. E. 1994, in Analysis of Interplanetary Dust, AIP Conf. Proc. 310 (eds., M. E. Zolensky, T. L. Wilson, F. J. M. Rietmeijer, & G. J. Flynn), AIP Press, New York, 245-254.

SOURCES OF 10 MICRON INTERPLANETARY DUST: THE CONTRIBUTION FROM THE KUIPER BELT

G. J. Flynn
Dept. of Physics, SUNY-Plattsburgh, Plattsburgh, NY 12901

Abstract. Two major sources are observed to contribute to the Zodiacal Cloud: main-belt asteroids and active comets. However, the discovery of 100 km size objects in trans-Neptunian orbits (Jewitt and Luu 1993) coupled with Pioneer 10 measurements showing an essentially constant flux of 10 μm dust from 4 to 18 AU with indications that dust may be in near-circular orbits (Humes 1980) suggests that collisions in the Kuiper Belt may contribute significantly to the Zodiacal Cloud and to the interplanetary dust collected from the Earth's stratosphere. Kuiper Belt dust collected at Earth could be identified by high densities of solar flare tracks, unusually thick amorphous rims, and high concentrations of spallogenic isotopes.

1. Introduction

Dust particles are removed from interplanetary space by Poynting-Robertson drag (P-R drag) and by catastrophic collisions on time scales that are short compared to the age of the solar system. Thus, a recent source is required to produce the current interplanetary dust complex. In principle every solar system object can contribute to the interplanetary dust cloud by processes such as outgassing, erosion, catastrophic collisions, tidal disruption, and volcanism. However, active comets and main-belt asteroids are assumed to be the major contributors to the Zodiacal Cloud because of the infrared observations of dust trails or dust bands associated with these sources.

2. Constraints on the Sources

Dermott et al. (1994), from detailed modeling of the infrared dust bands, find that the main-belt asteroids contribute about 30% of the dust to the Zodiacal Cloud. The remainder of the cloud requires a source with a higher mean inclination to the ecliptic. Dermott et al. (1994) suggest active comets are the likely source for the remaining 70% of the Zodiacal dust. However, Flynn (1992) pointed out that a cometary source of this magnitude should result in catastrophic collision lifetimes for large (>200 μm) micrometeorites which are too short to allow their survival during transport by P-R drag from the main-belt to the Earth. The collection of large micrometeorites having cosmic ray exposure durations consistent with a main-belt asteroidal origin (Nishiizumi et al. 1991) suggests the contribution of active comets to the Zodiacal Cloud is significantly smaller than 70% of the total (Flynn 1992).

Taken together these results suggest a third contributor to the Zodiacal Cloud which provides dust in nearly circular orbits but with a larger range of inclinations than the dust provided by main-belt asteroids, and which is undetected by satellite infrared measurements, presumably because of its large heliocentric distance. Debris produced by collisions in the Kuiper Belt would meet these criteria (Flynn 1994).

3. Evidence From the Pioneer Spacecraft

The Pioneer 10 and Pioneer 11 spacecraft detected dust particles out to about 18 AU (Humes 1980), where the dust detectors ceased to function. This direct measurement of interplanetary dust with masses $>8\times10^{-10}$ grams (~9 μm diameter) by Pioneer 10 and $>6\times10^{-9}$ grams (~18 μm diameter) by Pioneer 11 provides observational evidence of the orbital properties of the dust and constraints on its major sources. The Pioneer measurements have been interpreted to indicate that:

1) a large fraction of the dust at 1 AU is in near-circular orbits (Humes 1974),

2) a large fraction of the dust near Jupiter (5.2 AU) and Saturn (9.5 AU) may be in near-circular heliocentric orbits (Humes 1980), and,

3) that the rate of dust impacts does not diminish significantly after passage through the main-belt, remaining roughly constant out to 18 AU (Humes 1980).

The first two observations suggest active comets are not the dominant source of interplanetary dust, since the eccentricities of the orbits of cometary dust particles are still significant at 1 AU (Flynn 1989; Jackson & Zook 1992). The third observation suggests main-belt asteroids are not the dominant source of interplanetary dust, since P-R drag would cause the orbits of 10 μm dust produced in the main-belt to evolve rapidly inward, resulting in a sharp drop in the dust detection rate outside of the main-belt. The Pioneer measurements are consistent with a significant dust source at a heliocentric distance >>4 AU, producing interplanetary dust in near-circular orbits.

4. A Kuiper Belt Source of the Pioneer 10/11 Dust

The discovery by Jewitt and Luu (1993) of large objects (>100 km) in trans-Neptunian, heliocentric orbits possibly provided the first detection of the Kuiper Belt, the proposed source for short-period comets. Jewitt and Luu (1995) identified 24 trans-Neptunian objects, and estimated the number of undetected objects >100 km as $\sim10^4$. A Hubble Space Telescope search for smaller objects identified 29 Kuiper Belt objects of ~10 km diameter, with an estimated total population of $\sim2\times10^8$ such objects within 40 AU and having inclinations up to 12° (Cochran et al. 1995). Collisions between these objects should result in significant dust production in the Kuiper Belt.

Once the size-frequency distribution and the spatial density of the objects in the Kuiper Belt are established, the dust production rate from collisions within the belt can be modeled. At present, we can use the Pioneer measurements to estimate the contribution at Earth from the dust detected at 18 AU.

5. Modeling the Pioneer 10 and 11 Flux at Earth

Since the Pioneer spacecraft detected a relatively constant flux of dust from 4 to 18 AU (except near Jupiter and Saturn), the simplest model of the terrestrial contribution from the dust detected at 18 AU assumes that there is no significant sink for this dust inside of 4 AU, and the flux remains constant to 1 AU. An obvious mechanism for a dust sink would be vaporization, if the meteoroids were made predominantly of ices.

In the absence of a sink, the contribution from the dust detected at 18 AU to the flux of dust particles having masses $>8\times10^{-10}$ grams at Earth would be 2×10^{-6} particles/m^2-sec. Since the total flux of micrometeoroids $>10^{-9}$ grams measured in low-Earth orbit, on the Long Duration Exposure Facility, is 1×10^{-3} particles/m^2-sec (Love and Brownlee 1993), the particles detected by Pioneer 10 at 18 AU could contribute ~20% of the total ~10 μm diameter interplanetary dust at Earth.

This simple model overlooks four important considerations:

Appendix N:
Flynn, George
SUNY Plattsburgh - 62
Appendix N: Flynn, G.J. (1996) Sources of the 10 Micron Interplanetary Dust: The Contribution from the Kuiper Belt, IAU Symposium, 150, in press.

1) the expected increase in spatial density with decreasing heliocentric distance for particles evolving into the Sun under the influence of only P-R drag and solar gravity,

2) gravitational focusing which increases the effective capture cross-section,

3) particle loss by gravitational interactions with Jupiter and Saturn, and,

4) particle loss (or production) by catastrophic collisions.

The first two factors increase the dust flux at Earth, while the last two decrease the flux over that measured at 18 AU. Liou et al. (1995) have modeled the orbital evolution of small dust particles from the Kuiper Belt. They found that gravitational scattering by the gas giant planets ejects about 80% of these particles from the solar system, while the remaining 20% reach 1 AU with relatively low orbital eccentricities.

Assuming: 1) an 80% loss of dust encountering the gas giants, 2) an Earth encounter velocity of 5 km/sec, and 3) orbital evolution under the influence of P-R drag, the particles detected by Pioneer 10 at 18 AU should contribute 2×10^{-5} particles/m^2-sec at Earth, which exceeds the measured terrestrial flux of particles $>10^{-9}$ grams by a factor of 2. This clearly overestimates the actual contribution.

Liou et al. (1996) point out that dust grains >4 μm in diameter have a high probability of loss by catastrophic collisions with interstellar dust while evolving from 40 AU into the inner solar system. The relatively constant dust flux measured by Pioneer 10 from 18 AU to 4 AU suggests significant particle loss (by collisions or by planetary scattering), since orbital modeling using only P-R drag indicates the flux should increase by about an order-of-magnitude from 18 AU to 4 AU. However the Pioneer data also demonstrates that, unless there are additional dust sources between 18 AU and 4 AU, a significant fraction (~10%) of the ~10 μm dust detected at 18 AU survives to reach 4 AU.

6. Identification of IDPs From the Kuiper Belt

Ten micron diameter IDPs of density 2 gm/cm^3 which originate in the Kuiper Belt (~40 AU) and spiral inward under P-R drag without experiencing either fragmentation or trapping in a gravitional resonance reach 1 AU in ~1×10^7 years, compared to ~6×10^4 years for similar particles spiraling from the main-belt to 1 AU. The duration of space exposure for cometary IDPs depends on the initial orbit, but the space exposure ages of typical 10 μm cometary IDPs range from 3×10^4 years (d'Arrest) to 11×10^4 years (Swift-Tuttle) (Flynn 1989). Thus, IDPs from the Kuiper Belt experience significantly greater effects of space exposure than do main-belt asteroidal or cometary IDPs. The effects of space exposure are the production of nuclear damage tracks, amorphous rims on exterior surfaces, and cosmogenic nuclides.

Nuclear damage tracks, imaged in the Transmission Electron Microscope (TEM), are seen in the crystaline phases of IDPs recovered from the Earth's stratosphere. The track densities are generally consistent with the space exposure received in traveling from the main-belt to the Earth under P-R drag (Sandford & Bradley 1990). Assuming: 1) a $1/r^2$ falloff of solar flare Fe-ion flux with heliocentric distance, 2) orbital evolution dominated by P-R drag, and 3) no particle fragmentation enroute, the track density in an IDP originating in the Kuiper Belt would exceed that in main-belt asteroidal IDPs of the same size and density by a factor of ~12.

Solar wind ions, which have energies of ~1 KeV/nucleon, are implanted to depths of tens of nanometers in crystals exposed on the lunar surface. This produces amorphous, radiation damaged rims typically ~30 nm thick (Bibring et al. 1972). Similar amorphous rims, with thicknesses up to 50 nm, are seen on the exposed surfaces of olivine and pyroxene grains on the exterior of IDPs (Bradley & Brownlee 1986). Higher energy solar particles, ≥10 KeV/nucleon, are less abundant, but given

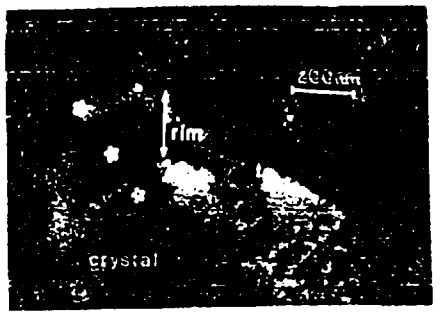

Figure 1. TEM image of one edge of W7027 C4, a 12 micron interplanetary dust particle (IDP) collected from the Earth's stratosphere, which has an order-of-magnitude higher solar flare track density (dark, linear features in the crystal) and a much thicker amorphous rim (~200 nm) than do typical IDPs. (Photo by J. P. Bradley.)

long exposure times (>100,000 years) these solar energetic particles should produce amorphous rims 150 to 250 nm thick (Christopherson and McKay 1995). Thus, IDPs from the Kuiper Belt should have amorphous rims ~250 nm thick, about a factor of 5 thicker than the rims on IDPs from main-belt asteroids or from typical active comets. Solar cosmic rays are produced by galactic and solar cosmic rays. Kuiper Belt IDPs would receive ~300 times the integrated dose from galactic cosmic rays and ~12 times the integrated dose from solar cosmic rays as do IDPs from the main-belt.

Bradley has identified one IDP, out of about 50 examined in detail, with a solar flare track density about an order-of-magnitude higher and a sputtered rim about a factor of 5 thicker than found in typical IDPs (J. P. Bradley Pers. Comm. 1995). This particle, shown in Figure 1, is a strong candidate for a Kuiper Belt IDP. However, any single IDP might be trapped in a planetary gravitational resonance long enough to receive this irradiation, thus detailed modeling of resonance trapping durations and probabilities, as well as the identification of additional IDPs with indications of long space exposures, will be required to convincingly identify IDPs from the Kuiper Belt.

References

Bibring, J. P. et al. 1972, Science, 175, 753-755.
Bradley, J. P. & Brownlee, D. E. 1986, Science, 231, 1542-1544.
Christopherson, R. & McKay, D. 1995, Lunar & Planetary Science XXVI, 245-246.
Cochran, A. L., Levison, H. F., Stern, S. A., & Duncan, M. J. 1995, "The Discovery of Halley-sized Kuiper Belt Objects Using HST," Ap. J., in press.
Dermott, S. F. et al. 1994, in Asteroids, Comets, and Meteors 1993, 153-156.
Flynn, G. J. 1989, Icarus, 77, 287-310.
Flynn, G. J. 1992, in Asteroids, Comets, and Meteors 1991, 195-199.
Flynn, G. J. 1994, Lunar & Planetary Science XXV, 379-380.
Humes, D. H. 1971, J. Geophys. Res., 79, 3677-3684.
Humes, D. H. 1980, J. Geophys. Res., 85, 5841-5852.
Jackson, A. A. & Zook, H. A. 1992, Icarus, 97, 70-84.
Jewitt, D. & Luu, J. 1993, Nature, 362, 730-732.
Jewitt, D. & Luu, J. 1995, Astron. J., 109, 1867-1876.
Liou, J. C. et al. 1995, Lunar & Planetary Science XXVI, 853-854.
Liou, J. C. et al. 1996, "The Contribution of Kuiper Belt Dust Grains to the Inner Solar System," these proceedings.
Love, S. G. & Brownlee, D. E. 1993, Science, 262, 550-553.
Nishiizumi, K. et al. 1991, Earth and Planet. Sci. Lett., 104, 315-324.
Sandford, S. A. & Bradley, J. P. 1990, Icarus, 82, 146-166.